

Nonlinear ENSO Warming Suppression (NEWS)

TSUBASA KOHYAMA AND DENNIS L. HARTMANN

Department of Atmospheric Sciences, University of Washington, Seattle, Washington

(Manuscript received 25 July 2016, in final form 26 December 2016)

ABSTRACT

In global warming experiments, the majority of global climate models warm faster in the eastern equatorial Pacific than in the west and produce a weakening of the Walker circulation. In contrast, GFDL-ESM2M is an exception that exhibits a La Niña-like mean-state warming with a strengthening of the Walker circulation. This study explores the cause of this exceptional response and proposes a new mechanism, the nonlinear ENSO warming suppression (NEWS), where the transient heating rate difference between the atmospheric and oceanic reservoirs annihilates extreme El Niños, causing a suppression of mean-state warming in the east. Heat budget analyses of GFDL-ESM2M robustly show that nonlinear dynamical heating, which is necessary for extremely warm El Niños, becomes negligible under warming. An idealized nonlinear recharge oscillator model suggests that, if the temperature difference between the atmospheric and oceanic reservoirs becomes larger than some threshold value, the upwelling becomes too efficient for El Niño–Southern Oscillation (ENSO) to retain its nonlinearity. Therefore, extreme El Niños dissipate but La Niñas remain almost unchanged, causing a La Niña-like mean-state warming. NEWS is consistent with observations and GFDL-ESM2M but not with the majority of state-of-the-art models, which lack realistic ENSO nonlinearity. NEWS and its opposite response to atmospheric cooling, the nonlinear ENSO cooling suppression (NECS), might contribute to the Pacific multidecadal natural variability and global warming hiatuses.

1. Introduction

The tropical Pacific Ocean is one of the main contributors to variability in Earth's climate system, but whether the mean-state sea surface temperature (SST) response of this region to global warming should be El Niño-like (SST warms faster in the east) or La Niña-like (SST warms faster in the west) is uncertain from the perspective of observations (Rayner et al. 2003; Smith et al. 2008; Christensen et al. 2013), models (Knutson and Manabe 1995; Cane et al. 1997; Vecchi and Soden 2007; Kim et al. 2014), and theory (Clement et al. 1996; Collins et al. 2005, 2010; Xie et al. 2010; Held et al. 2010; An et al. 2012). In this study we use the terms “El Niño like” and “La Niña like” owing to their lucidity and simplicity, but it is controversial whether it is appropriate to use them to describe the tropical SST response to warming. This controversy is because these terms are associated with El Niño–Southern Oscillation (ENSO), a dominant interannual natural climate mode that modulates the SST deviations from the tropical Pacific mean state, which

may not necessarily be similar to a forced global warming response (Collins et al. 2010). In global warming projections, however, it is extremely important to understand possible processes that determine the mean-state changes in this region and to narrow their major uncertainties because the tropical Pacific mean-state variability and its changes are expected to have substantial scientific and societal impacts on not only the tropics and subtropics (e.g., droughts, floods, heat waves, poor harvests, and changing marine ecosystems) but also the midlatitudes and high latitudes (e.g., cold spells, changing tropical cyclone genesis frequency, and modulating Antarctic sea ice trends) (Yokoi and Takayabu 2009; Murakami et al. 2012; Christensen et al. 2013; Kohyama and Hartmann 2016).

The vast majority of the state-of-the-art global climate models (GCMs) that participated in phase 5 of the Coupled Model Intercomparison Project (CMIP5) exhibit El Niño-like mean-state responses to global warming. These responses are widely believed to be associated with a weakening of the Walker circulation, which some believe is necessary to sustain the global-mean water and energy balance derived by Held and Soden (2006). This necessity was supported by the

Corresponding author e-mail: Tsubasa Kohyama, kohyama@uw.edu

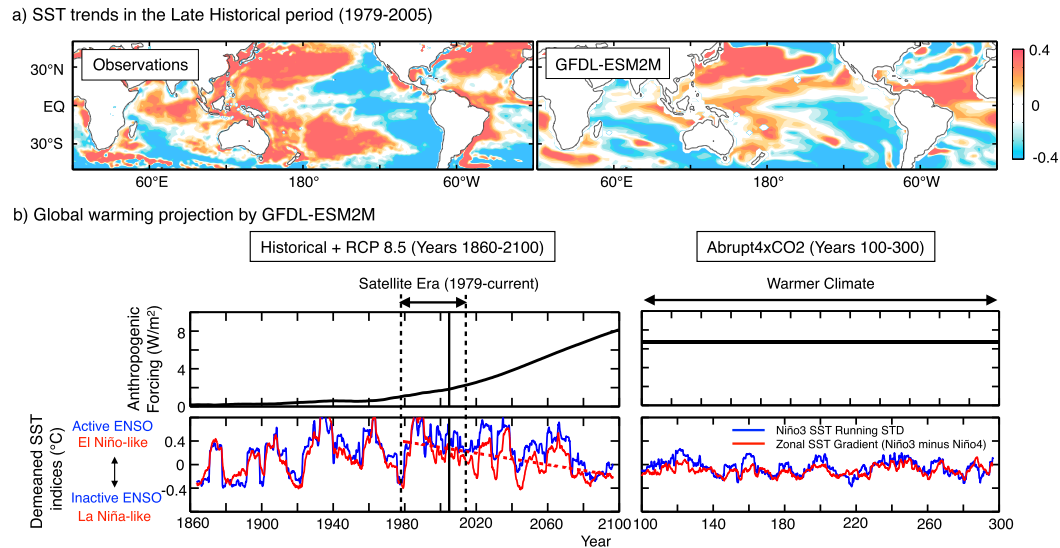


FIG. 1. (a) Observed and modeled SST trends ($^{\circ}\text{C century}^{-1}$) computed relative to the tropical Pacific mean trends (30°S – 30°N , 90°E – 60°W) during the late historical period. Blue colors denote a warming slower than the tropical Pacific mean, not necessarily a cooling. (b) The top panels show the strength of anthropogenic forcing for the historical, RCP8.5, and abrupt4xCO₂ runs. For abrupt4xCO₂, only after year 100 is shown because it takes several decades before the system reaches its quasi equilibrium. The equilibrated value of the anthropogenic forcing in the abrupt4xCO₂ run (6.72 W m^{-2}) is estimated by Andrews et al. (2012). The bottom panels of (b) show the 7-yr running standard deviations (RSTD) of SST (blue line) averaged over the Niño-3 region (5°S – 5°N , 150° – 90°W). RSTD is calculated to represent deviations from the running mean state at each window. Also shown is the observed zonal SST gradient (ZSG) index (red line) defined as the difference Niño-3 minus Niño-4 (5°S – 5°N , 160°E – 150°W) SST. A 7-yr running mean is applied. The dashed line shows the least squares best-fit line calculated from 1979–2100. Both indices are expressed relative to the means over the entire time span of piControl run (see also Fig. 8 of KHB17).

multimodel mean behavior of CMIP3 models as shown by Vecchi and Soden (2007). Recent work by Kohyama et al. (2017, hereafter KHB17), however, showed that GFDL-ESM2M (a GCM developed by the Geophysical Fluid Dynamics Laboratory) is an interesting exception in that it produces a well-defined La Niña-like mean-state warming with a clear strengthening of the Walker circulation.

Figure 1, which is reproduced from KHB17, shows the observed SST trends during the historical period (1979–2005) and the modeled SST response of GFDL-ESM2M in some global warming experiments. Using this model, whose ENSO representation is known to be reasonable (e.g., Bellenger et al. 2014), KHB17 made a case that the La Niña-like trend could be a physically consistent response to warming and that the forced response could have been detectable since the late twentieth century. This result may appear to be provocative to the research community because the recent La Niña-like trend has widely been believed to be the result of purely natural variability (e.g., Christensen et al. 2013). This belief, however, depends to a large extent on the evidence that the majority of the CMIP5 models exhibit El Niño-like warming patterns. In this sense, the previous studies may

have resorted to a “majority decision” among imperfect models. Of course, it is a hard task to determine whether this outlier, GFDL-ESM2M, captures the real world better than other models, so it may be early to determine this with certainty. It is, however, not too early to begin the analysis, since the tropical Pacific response to warming is one of the key uncertainties in climate projections that will have a substantial practical impact in the near term.

In addition, a remarkable structural resemblance of the strengthening Walker circulation between GFDL-ESM2M and observations during the satellite era (see Fig. 3 of KHB17) increases the interest in investigating this model further to determine whether this observed circulation change is purely due to natural multidecadal variability or partly a forced response to global warming. One might be concerned that this strengthening Walker circulation could violate the robust energy and water balance proposed by Held and Soden (2006). KHB17 showed that, however, the balance only constrains the global-mean change but not necessarily a regional response (e.g., the Walker circulation), so it is still possible to simulate a strengthening Walker circulation if the circulation weakens elsewhere. Comparing with GFDL-ESM2G, which

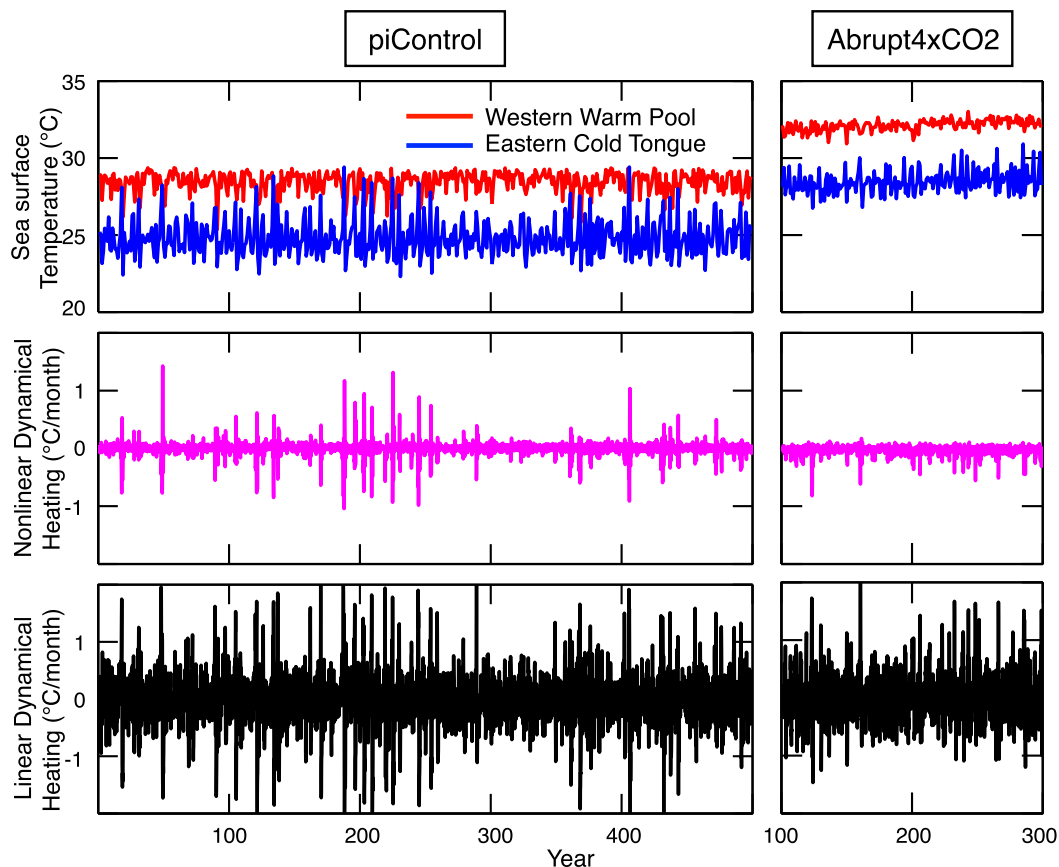


FIG. 2. (top) SST averaged over DJF, simulated by GFDL-ESM2M under piControl and abrupt4xCO₂ scenarios. Red curves show the SST time series averaged over the western warm pool (5°S–5°N, 130°–160°E), and the blue curves show those of the eastern cold tongue (5°S–5°N, 120°–90°W). For abrupt4xCO₂, only after year 100 is shown because it takes several decades before the system reaches its quasi equilibrium. (middle) NDH and (bottom) LDH time series calculated using Eq. (1) for the same model runs as in (top), averaged over 5°S–5°N, 170°E–100°W. A 3-month running mean is applied to both time series.

differs from GFDL-ESM2M only by its oceanic component, KHB17 suggested that an important oceanic mechanism might play a major role in controlling the mean-state SST warming response, which then determines the atmospheric circulation changes.

KHB17 also concluded that GFDL-ESM2M does a particularly good job of reproducing the observed correlation between the zonal SST gradient and the amplitude of ENSO and that its La Niña-like mean-state warming trend in response to warming may be causally related to the weakening ENSO amplitude (Fig. 1b). This hypothetical relationship is also consistent with a recent paper by Zheng et al. (2016), which showed that a group of four CMIP5 models with a La Niña-like warming shows a weakening of the ENSO amplitude. Therefore, we would like to understand why the ENSO in GFDL-ESM2M is weakened under a warmer climate. Figure 2, top, shows the SST during December–February (DJF) averaged over the western equatorial

warm pool region (5°N–5°S, 130°–160°E) and the eastern equatorial cold tongue (5°N–5°S, 120°–90°W), as in Fig. 1 of An and Jin (2004, hereafter AJ04) but for the pre-industrial control (piControl) and abrupt quadrupling of carbon dioxide (CO₂) (abrupt4xCO₂) runs defined by the CMIP5 project. Only the years after year 100 are shown for the abrupt4xCO₂ run because it takes a couple of decades before the climate reaches its quasi equilibrium after the abrupt CO₂ increase (not shown). The ENSO amplitude is substantially weakened in a warmer climate in GFDL-ESM2M, which is consistent with the result shown in KHB17.

More importantly, the SST time series of abrupt4xCO₂ show no extreme El Niño (EEN) events. Here, if the cold tongue SST closely approaches or surpasses the warm pool SST, then we refer to these El Niño events as EENs. In the observed record, the El Niños in 1982/83 and 1997/98 are classified as EENs as we will show later in this section. Jin et al. (2003) and AJ04 called the

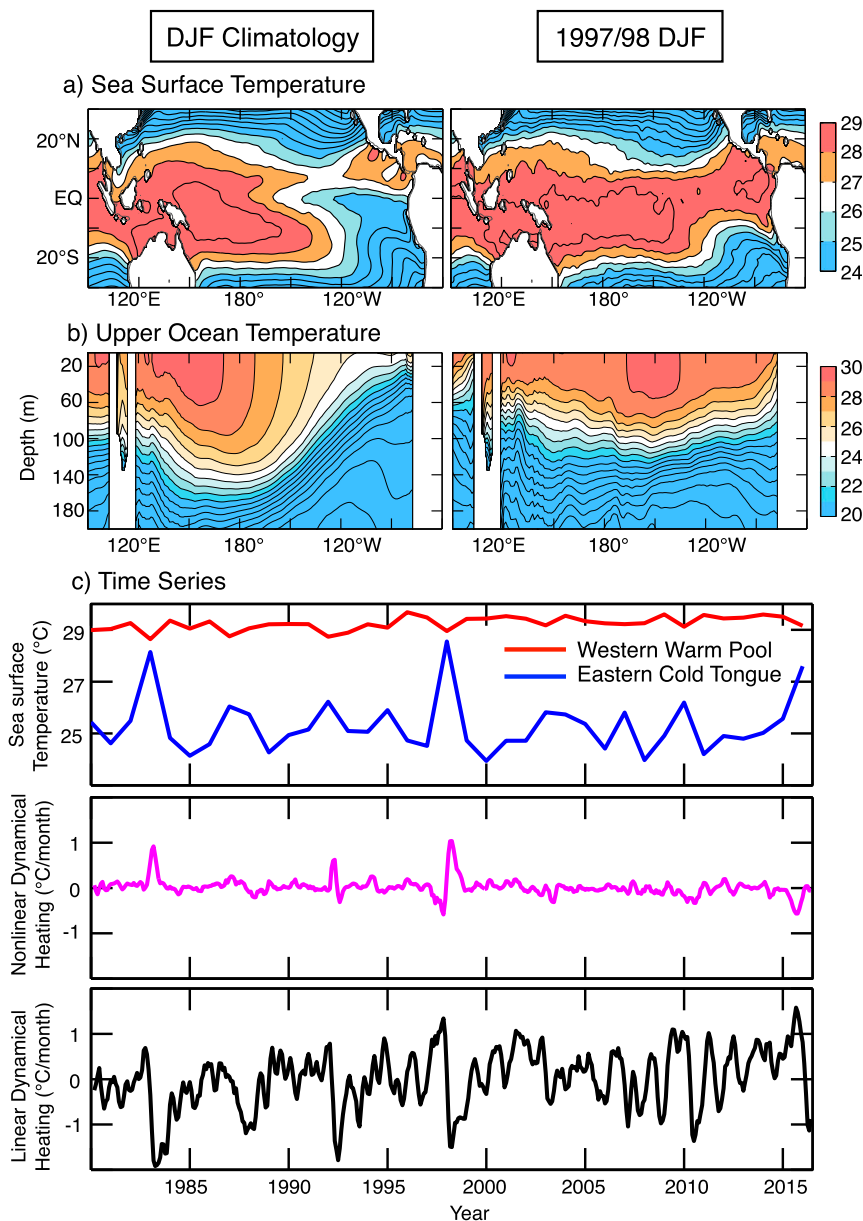


FIG. 3. (a) Left panel shows the observed SST climatology during DJF. Right panel of (a) as in the left panel, but for DJF 1997/98. Contour interval is 1°C. (b) As in (a), but for observed upper-ocean potential temperature. (c) As in Fig. 2, but for observations.

western warm pool SST “the upper bound” of the eastern cold tongue SST, defining this upper bound as the maximum potential intensity (MPI) of an El Niño. One of the main conclusions of Jin et al. (2003) and AJ04 is that, during EENs, the climatological conditions of the ocean and atmosphere are completely collapsed and that one cannot treat EENs as linear perturbations from the climatological mean. In Fig. 3, we have reproduced some figures shown in AJ04 but with a longer record. The SST spatial pattern during the EEN in

DJF 1997/98 shows a completely different structure than the climatological SST. Moreover, the equatorial upper-ocean temperature clearly shows that, during the EEN, the thermocline is almost flat across the equatorial Pacific. This is virtually the largest El Niño that can potentially occur, which is why AJ04 defined the warm pool SST as the MPI. The eastern equatorial SST is bounded by the MPI, and the MPI is, in turn, determined by the radiative–convective equilibrium temperature (Waliser and Graham 1993).

The next question, then, is whether the mechanisms that cause EENs and normal ENSO events are different. Jin et al. (2003) and AJ04 addressed this question by performing a heat budget analysis of the upper ocean by decomposing the dynamical heating terms into linear dynamical heating (LDH) and nonlinear dynamical heating (NDH). The heat budget of the mixed layer can be written in the form of the following equation:

$$\begin{aligned} \frac{\partial T'}{\partial t} = & \left(-u' \frac{\partial \bar{T}}{\partial x} - v' \frac{\partial \bar{T}}{\partial y} - w' \frac{\partial \bar{T}}{\partial z} - \bar{u} \frac{\partial T'}{\partial x} - \bar{v} \frac{\partial T'}{\partial y} - \bar{w} \frac{\partial T'}{\partial z} \right) \\ & + \left(-u' \frac{\partial T'}{\partial x} - v' \frac{\partial T'}{\partial y} - w' \frac{\partial T'}{\partial z} \right) + R', \end{aligned} \quad (1)$$

where t denotes time; x , y , and z denote the longitudinal, latitudinal, and vertical coordinates, respectively; T denotes the mixed layer temperature; and u , v , and w are zonal, meridional, and vertical velocities, respectively. Overbars denote the monthly climatological mean, and primes denote the deviations therefrom. Surface heat flux and subgrid-scale contributions are all included in the residual term R . AJ04 defined the terms in the first (second) parentheses as LDH (NDH).

Most important among the NDH terms is the vertical component. During El Niño events, anomalous downwelling tends to occur simultaneously with anomalously strong stratification; therefore, NDH warms the mixed layer. During La Niña events, however, anomalous upwelling occurs with anomalously weak stratification. In other words, the upwelling advects anomalously warm water from the bottom, so NDH again warms the mixed layer. Mathematically, the covariance between downwelling $-w'$ and the temperature gradient $\partial T'/\partial z$ remains positive in both El Niños and La Niñas. Hence, the resulting total dynamical heating flux (LDH + NDH) warms the surface a lot in El Niño events but cools the surface a little in La Niña events. This asymmetry helps explain why large SST anomalies in the cold tongue region are skewed toward warm events (i.e., EENs). In addition, as seen in the time series of MPI, the cold tongue SST, NDH, and LDH calculated for the uppermost 50 m in Fig. 3c, LDH is always important, but NDH is comparable to LDH only for EENs (i.e., 1982/83 and 1997/98).

Though the available observed record is short, it is suggestive that the NDH contribution is almost negligible after 1999. Interestingly, at least by this metric, the recent large El Niño in 2015/16 may not be classified an EEN, which is consistent with the fact that the El Niño in 2015/16 was the largest in historical record in terms of the Niño-3.4 index (SST averaged over

5°N–5°S, 170°–120°W) but not in terms of the Niño-3 index (5°N–5°S, 150°–90°W) (not shown). Though we are aware that the necessity of NDH for EENs remains an open question (e.g., Boulanger et al. 2004; Levine et al. 2016), we assume in this study that NDH is important for EENs, following what AJ04 suggested. This assumption is also based on what we have detected in the other EENs, the nonlinear ENSO theory, and the model outputs from GFDL-ESM2M introduced in this study.

Based on the observational evidence shown by AJ04, we hypothesize that, at least in GFDL-ESM2M, the reason why EENs are not detected in abrupt4xCO2 may be that NDH becomes unimportant in a warmer climate. The middle and bottom panels of Fig. 2 show the time series of NDH and LDH for the upper 50 m, respectively, for both piControl and abrupt4xCO2. As expected, NDH becomes much weaker in the warmer run, whereas LDH remains stationary to first order. This dominance of LDH means that ENSO in a warmer climate becomes almost linear, and the dissipation of NDH is a main contributor to the weakening ENSO amplitude in this model.

Hence, the questions we try to address in this paper are as follows: (i) Why does NDH become unimportant in a warmer climate in GFDL-ESM2M? (And, as a corollary, can we expect that fewer EENs will be observed in the future?) (ii) Can the weakening of the ENSO amplitude due to the weakening of NDH cool the mean-state SST of the cold tongue? (iii) Is the weakening ENSO amplitude a cause or an effect of the La Niña-like mean-state warming in GFDL-ESM2M (or neither)? (iv) Why does GFDL-ESM2M simulate these processes but other models do not? (What are the necessary conditions for simulating those processes? Are those processes realistic?) (v) Do these mechanisms also have implications for multidecadal natural variability? Despite some risk in exploring processes simulated by only a minority of models, we would like to understand why GFDL-ESM2M can be the minority in such a major property of GCMs. Considering its challenge as a scientific problem and its societal impact, the outcome is so important that we believe we must understand this intermodel difference better.

This article is organized as follows. The data and an idealized model used in this study are described in the next section. In section 3, the idealized model is used to explore why NDH becomes negligible in a warmer climate; furthermore, we confirm that these ideas are consistent with GFDL-ESM2M output. Then, in section 4, we further compare the idealized model, observations, and GFDL-ESM2M output to propose a

mean-state warming suppression mechanism as a forced response of the cold tongue to global warming. We also discuss the reason why only GFDL-ESM2M can simulate this mechanism, as well as the important difference between gradual and abrupt CO₂ increases. In section 5, we explore some implications of the above mechanism for multidecadal natural variability and global warming hiatuses. Conclusions are given in section 6.

2. Data and an idealized model

a. Data

Observed monthly SSTs are from the Hadley Centre Sea Ice and Sea Surface Temperature (HadISST) dataset (Rayner et al. 2003; available online at <http://www.metoffice.gov.uk/hadobs/hadisst/index.html> for the period 1880 through 2015). We use SST data from the period 1965 through 2015 (except Fig. 13), during which we expect the data to be less influenced by limited data sampling, changing measurement techniques, and analysis procedure dependence (Christensen et al. 2013). Whenever we show time series, we add the data of the first half of 2016 so that we do not miss the 2015/16 El Niño. The spatial resolution is 1° latitude × 1° longitude. Oceanic potential temperature and horizontal velocity reanalysis data are obtained from the National Centers for Environmental Prediction (NCEP) Global Ocean Data Assimilation System (GODAS) (Behringer and Xue 2004; available online at <http://www.esrl.noaa.gov/psd/data/gridded/data.godas.html>). The horizontal resolution is 1° longitude × 1/3° latitude, with a vertical resolution of 10 m for uppermost 230 m (no data deeper than 230 m are used in this study). The oceanic vertical motion at the 50-m depth is calculated assuming mass continuity with negligible density tendency, which exhibits very good agreement with vertical motion data available at the NCEP GODAS website. This agreement confirms the validity of this assumption and the algorithms we use for the model output described later.

We have used the representative concentration pathway (RCP) calculations and data (Meinshausen et al. 2011; available online at <http://www.pik-potsdam.de/~mmalte/rcps>). (The time series presented in Fig. 10 is the RCP8.5 anthropogenic forcing from 1860 through 2100.) In addition, annual-mean global-mean observed surface temperature is downloaded from the Goddard Institute for Space Studies (GISS) Surface Temperature Analysis (GISTEMP) (Hansen et al. 2010) produced by the GISTEMP Team 2016 at the National Aeronautics and Space Administration (NASA) Goddard Institute for Space Studies. (The

data were accessed on 7 July 2016 online at <http://data.giss.nasa.gov/gistemp/> and used to make Fig. 13.)

The surface temperature, oceanic potential temperature, and horizontal velocity output from GFDL-ESM2M are taken from the GFDL data portal (<http://nomads.gfdl.noaa.gov:8080/DataPortal/cmip5.jsp>). The experiments considered in this study are the first ensemble member of the piControl, historical, abrupt4xCO₂, 1% yr⁻¹ increase in CO₂ (1pctCO₂), RCP6.0, and RCP8.5 runs. At each depth, the oceanic variables are regridded via linear interpolation onto a 2.5° longitude × 2° latitude grid; the oceanic data have a vertical resolution of 10 m for the uppermost 230 m. The oceanic vertical motion at 50-m depth is calculated using the same procedure as described above. We also use other CMIP5 (Taylor et al. 2012) model output available at the Program for Climate Model Diagnosis and Intercomparison website (available online at <https://pcmdi.llnl.gov/projects/cmip5/>).

An important caveat of this study is that our results from GFDL-ESM2M are based on a single ensemble member for each experiment. In principle, we should test our results using multiple ensembles, but at the time of this writing, only a single ensemble member is available for each experiment of GFDL-ESM2M at the GFDL data portal. Nevertheless, by analyzing the piControl (500 yr), historical (146 yr), RCP6.0 (95 yr), RCP8.5 (95 yr), 1pctCO₂ (200 yr), and abrupt4xCO₂ (300 yr) runs, it turns out it is virtually certain that the nonlinear ENSO in this model is forced to weaken by global warming and that the warming response of the mean-state zonal SST gradient in this model is La Niña-like, at the very least. These relatively robust warming responses of GFDL-ESM2M are the two main ingredients of the mechanism proposed in this study.

Using the aforementioned oceanic data, LDH and NDH of the mixed layer are calculated using Eq. (1) at each gridpoint, assuming that the mixed layer depth is fixed at 50 m. As in AJ04, we have confirmed that the results shown in this paper are not sensitive to the choice of the mixed layer depth and its variability. To calculate LDH and NDH, the monthly climatology (\bar{T} , \bar{u} , \bar{v} , and \bar{w}) is calculated as the mean over the entire record for each month, except that linear trends are also added in RCP8.5 because the mean-state climatology also warms in this run. The LDH and NDH time series are calculated as the regional average over 5°N–5°S, 170°–100°W, following AJ04. The oceanic reservoir temperature beneath the thermocline T_o is calculated as the temperature at 100 m below the thermocline (the thermocline depth is defined as the depth with the maximum vertical temperature gradient). The results are not sensitive to

this choice of depth (i.e., 100 m), unless it is too close to the thermocline where the temperature has a larger interannual variance.

b. Idealized model

We use an idealized nonlinear recharge oscillator model introduced by Jin (1998) and Timmermann et al. (2003) and its modified versions. This model is essentially a simplified, two-box approximation of the Cane–Zebiak model (Zebiak and Cane 1987). The tendency of the temperature of the oceanic mixed layer in the western warm pool T_1 and the eastern cold tongue T_2 are given by

$$\frac{dT_1}{dt} = -\alpha(T_1 - T_a) - \frac{u}{L/2}(T_2 - T_1) \quad \text{and} \quad (2)$$

$$\frac{dT_2}{dt} = -\alpha(T_2 - T_a) - \frac{w}{H_m}(T_2 - T_{\text{sub}}), \quad (3)$$

where $1/\alpha$ denotes a thermal damping time scale, T_{sub} denotes subsurface temperature, and u and w are eastward and upward oceanic velocities, respectively. The variables H_m and L are the mixed layer depth and the basin width, respectively. The variable T_a denotes the zonally uniform lower atmospheric reservoir temperature, but except for section 5, T_a is replaced by the radiative–convective equilibrium temperature T_r as in Jin (1998) and Timmermann et al. (2003):

$$T_a = T_r. \quad (4)$$

Both T_1 and T_2 are relaxed toward T_a by the first terms of Eqs. (2) and (3), and the second terms of Eqs. (2) and (3) express the zonal and vertical temperature advection, respectively. Then, the wind stress τ , u , and w are expressed as follows:

$$\tau = -\mu(T_1 - T_2)/\beta, \quad (5)$$

$$\frac{u}{L/2} = \varepsilon\beta\tau, \quad \text{and} \quad (6)$$

$$\frac{w}{H_m} = -\zeta\beta\tau, \quad (7)$$

where μ is the sensitivity of the trade wind to the zonal SST gradient, and ε and ζ are zonal advection and upwelling efficiency (i.e., sensitivities of zonal and vertical oceanic currents to the trade wind), respectively. Parameterization of T_{sub} is given by Jin (1996) as follows:

$$T_{\text{sub}} = T_a - \frac{T_a - T_o}{2} \left(1 - \tanh \frac{H + h_2 - z_0}{h^*} \right), \quad (8)$$

where T_o is the oceanic reservoir temperature beneath the thermocline, h_2 is the departure of the eastern thermocline depth from the reference depth H , z_0 is the depth at

which w takes its characteristic values, and h^* is a scale parameter that controls the sharpness of the thermocline. The thermocline depth departure h_1 (west) and h_2 (east) follow the recharge oscillator (Jin 1997) formulations:

$$\frac{dh_1}{dt} = -rh_1 - \left(\frac{rbL}{2} \right) \tau \quad \text{and} \quad (9)$$

$$h_2 = h_1 + bL\tau, \quad (10)$$

where $1/r$ denotes the damping time scale of the anomaly, and b is the sensitivity of the thermocline to the trade wind change due to the Sverdrup transport. The parameter values used in this study follow AJ04 ($\alpha = 1/180 \text{ day}^{-1}$, $r = 1/400 \text{ day}^{-1}$, $H_m = 50 \text{ m}$, $H = 100 \text{ m}$, $z_0 = 75 \text{ m}$, $h^* = 62 \text{ m}$, $\mu = 0.0026 \text{ K}^{-1} \text{ day}^{-1}$, $\mu bL/\beta = 22 \text{ m K}^{-1}$, $\zeta = 1.3$, $\varepsilon = 0.11$, and $L = 15 \times 10^6 \text{ m}$) except for some modifications described below.

Timmermann et al. (2003) and AJ04 introduced $T_r(T_a)$ and T_o as constant parameters equaling 29.5° and 16°C , respectively. Here, to simulate the change of the radiative–convective equilibrium temperature and the reservoir temperature associated with global warming, we modify T_r and T_o to be simple linear functions of time:

$$\frac{dT_r}{dt} = Q_r \quad \text{or} \quad T_r = Q_r t + T_C \quad \text{and} \quad (11)$$

$$\frac{dT_o}{dt} = Q_o \quad \text{or} \quad T_o = Q_o t + T_D, \quad (12)$$

where Q_r , Q_o , T_C , and T_D are test parameters that will vary in the following sections. One of the main ideas presented in this paper is that $T_a - T_o (= T_r - T_o$ except for section 5) is a key parameter that determines the prominence of NDH and EENs. In “fixed reservoir temperature difference” experiments, we set $Q_r = Q_o = 0$, and in “increasing reservoir temperature difference” experiments, we set $Q_r > Q_o > 0$.

In section 5, we further generalize the idealized model, particularly Eq. (4), so that T_a becomes capable of responding to the eastern equatorial mean-state multidecadal variability. As shown in Kosaka and Xie (2013) and many others, a La Niña–like mean climate generally enhances the atmospheric cooling by the eastern equatorial Pacific, leading to global warming hiatuses or slowdowns. An El Niño–like mean state, on the other hand, suppresses the atmospheric cooling rate. Therefore, the tendency of T_a and its heating rate R_a are expressed as the following equations:

$$\frac{dT_a}{dt} = R_a \quad \text{and} \quad (13)$$

$$\frac{dR_a}{dt} = -\omega^2(T_a - T_r) - \gamma(T_a - T_2), \quad (14)$$

where γ denotes the sensitivity of atmospheric heating rate to the cold tongue SST, and ω is a normal-mode angular frequency of generalized multidecadal atmospheric natural variability that restores the atmospheric temperature toward radiative–convective equilibrium. This natural variability could be a synthesized effect of, for instance, the Planck feedback, water vapor feedback, ice–albedo feedback, cloud feedback, and so on. Therefore, the restoring effect expressed as the first term in Eq. (14) is not a simple relaxation that involves only negative feedbacks; rather, it excites an oscillatory behavior that involves both positive and negative feedbacks. The second term expresses a forcing by the eastern equatorial Pacific that cools the atmosphere, and we try to understand the atmospheric temperature variability as a forced oscillation. In this configuration, we could interpret Eq. (4) as a limit of infinitesimal atmospheric sensitivity to the Pacific cold tongue ($\gamma = 0$) and infinitesimally low frequency of the atmospheric normal mode ($\omega = 0$) with initial conditions of $T_a(t = 0) = T_c$ and $R_a(t = 0) = Q_r$. The parameter values are tuned to $\gamma = 0$ (zero sensitivity experiments) or $2 \times 10^{-9} \text{ day}^{-2}$ (i.e., $1/13700 \text{ yr}^{-2}$) (nonzero sensitivity experiments) and $\omega = 2\pi/90 \text{ rad yr}^{-1}$ so that the model realistically simulates the phenomena of interest.

Following Timmermann et al. (2003), the above idealized model is integrated forward in time using a Runge–Kutta method of fourth order with a time step of 1 day. The results presented in section 3 and 4 are not sensitive to initial conditions if realistic initial conditions are chosen. In section 5, however, because of the more complicated model configuration, the range of initial conditions that reproduce our results appears to be narrower. In our study, we have used the initial conditions of $T_1 = 27^\circ\text{C}$, $T_2 = 20^\circ\text{C}$, $h_1 = 70 \text{ m}$, $T_a = T_r = 29.5^\circ\text{C}$, $T_o = 15^\circ\text{C}$, and $R_a = 0^\circ\text{C century}^{-1}$ at $t = 0$.

3. Dissipation of NDH and EEN events due to an increasing temperature difference between the atmospheric and oceanic reservoirs

In this section, we first use the idealized nonlinear recharge oscillator model to obtain some ideas for why NDH becomes unimportant in warmer runs of GFDL-ESM2M. Then, we further analyze the output from GFDL-ESM2M to show that the idealized model captures the behavior of GFDL-ESM2M reasonably well.

a. Key parameter $T_a - T_o$

Figure 4a shows MPI (i.e., warm pool SST T_1), the cold tongue SST T_2 , and the NDH time series simulated by the idealized model with fixed reservoir temperature difference $T_a - T_o = 12.0^\circ, 13.9^\circ, 14.1^\circ, \text{ and } 14.3^\circ\text{C}$. Here

we fix $T_a = 29.5^\circ\text{C}$ and vary T_o to realize different values of $T_a - T_o$, but we obtain nearly identical results if we fix T_o and change T_a instead. As Timmermann et al. (2003) showed by changing either the zonal advection ε or upwelling efficiency ζ , some different regimes of the ENSO variability are identifiable. The regime with $T_a - T_o = 12.0^\circ\text{C}$ corresponds to a regime with strong zonal advection, where all ENSO events are EENs (i.e., the cold tongue SST always reaches the MPI). As $T_a - T_o$ becomes larger ($T_a - T_o = 13.9^\circ\text{C}$), the frequency of EENs decreases with lengthening, intermittent linear periods in between EENs, whose basic dynamics can be explained by the linear recharge oscillator system. Then, the intervals between EENs become longer and irregular at $T_a - T_o = 14.1^\circ\text{C}$, and the EENs finally vanish at the regime $T_a - T_o = 14.3^\circ\text{C}$. In this last regime, the ENSO becomes completely linear and no EENs are detected. These four experiments are consistent with observations that NDH is only important for EENs as shown in Fig. 3c and by AJ04.

Based on the results obtained from the fixed reservoir temperature difference runs, we surmise that a “threshold reservoir temperature difference” at which the importance of NDH bifurcates exists between 14.1° and 14.3°C . To test this idea, we have performed an increasing reservoir temperature difference run, where we gradually increase the $T_a - T_o$ linearly in time. As an analog for global warming, we have simulated the increasing temperature difference by setting different heating rates, $Q_r = 1^\circ\text{C century}^{-1}$ and $Q_o = 0.3^\circ\text{C century}^{-1}$, for the atmospheric and oceanic reservoirs, respectively. Figure 4b shows the result of this run, and, as expected, the intervals between the EENs become gradually longer (from about 12- to 18-yr intervals) as the system warms, and the system exhibits no EENs and NDH after $T_a - T_o$ surpasses 14.2°C in year 100.

Mathematically, it is easy enough to understand why the system exhibits the same regime shift as the one shown in Timmermann et al. (2003). In their Fig. 6, for a given efficiency of zonal advection ε , they varied the efficiency of upwelling ζ with T_a and T_o fixed, whereas we have varied $T_a - T_o$ with ζ fixed. It turns out that varying $T_a - T_o$ yields essentially the same effect as changing the upwelling efficiency ζ . Because variations of $T_a - T_o$ only influence Eq. (8), the increase of $T_a - T_o$ means a decrease of T_{sub} , or an increase of $(T_2 - T_{\text{sub}})/H_m$ (vertical temperature gradient) in Eq. (3). Because $(T_2 - T_{\text{sub}})/H_m$ is multiplied by $w = -\zeta\beta\tau H_m$ in Eq. (3), it is evident that increased $T_a - T_o$ has the same effect on the tendency of T_2 as increased ζ .

Physically, the above mathematical explanation can be translated as follows. If global warming heats the lower atmosphere faster than the ocean interior beneath

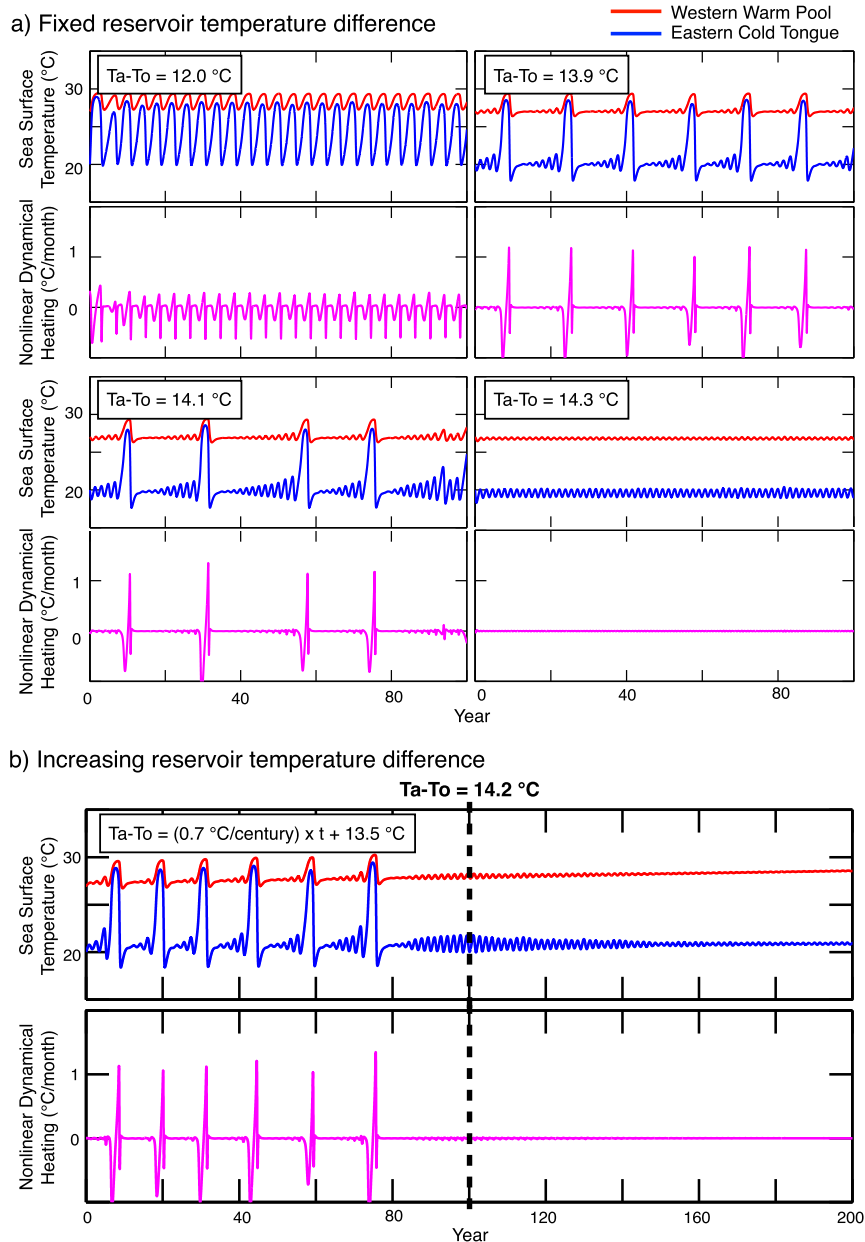


FIG. 4. (a) As in the top and middle panels of Fig. 2, but with the idealized model. Each panel shows a simulation with fixed temperature difference between the atmospheric and oceanic reservoir $T_a - T_o$, indicated in the rectangle at the top left. (b) As in (a), but increasing $T_a - T_o$ following the equation shown in the rectangle at the top left. The dashed line shows the time when $T_a - T_o$ reaches the threshold that bifurcates the importance of the ENSO nonlinearity.

the thermocline, it tends to enhance the upper-ocean stratification, which in turn enhances the mixed layer cooling by the equatorial upwelling. Hence, this overwhelming upwelling prevents the thermocline from recharging the heat enough to collapse its climatological mean structure. This “rigid” climatological thermocline means a complete damping of NDH, making it difficult

for a warm SST anomaly to mature in response to westerly wind anomalies (see also the schematics in Figs. 10a,b).

b. Comparison with GFDL-ESM2M

In state-of-the-art GCMs and in the real world, the lower-atmospheric temperature should warm faster

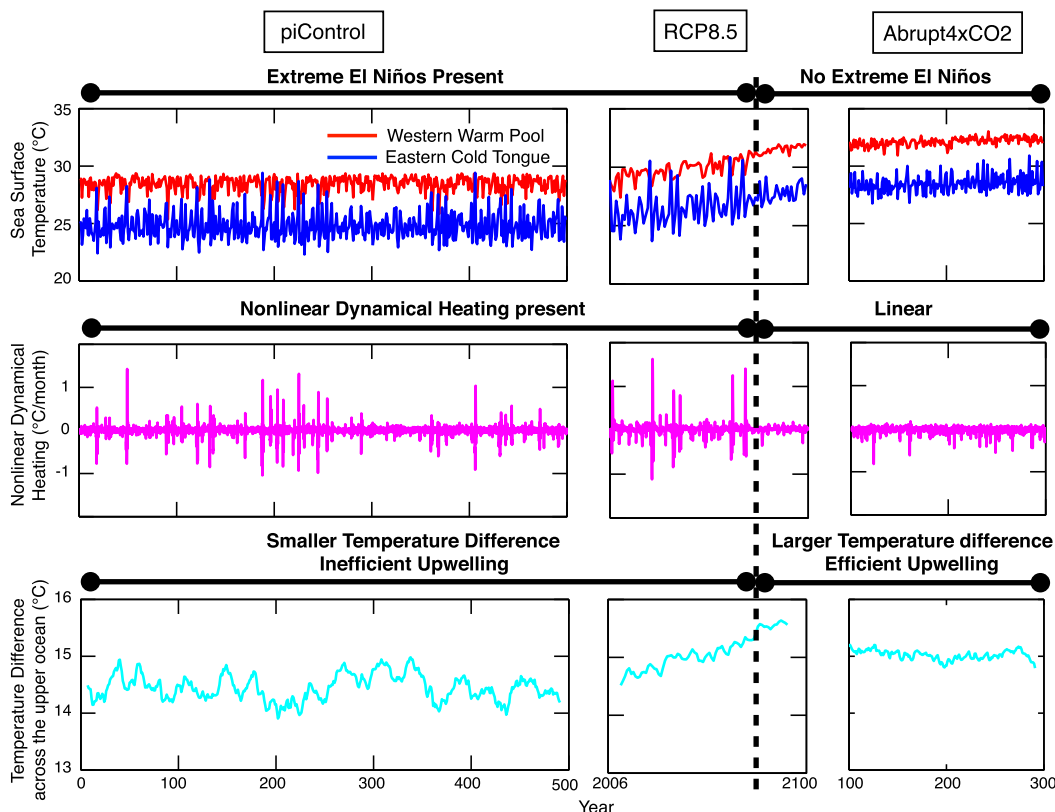


FIG. 5. As in the top and middle panels of Fig. 2, but with the RCP8.5 scenario inserted between piControl and abrupt4xCO2. The scale of the horizontal axes for RCP8.5 is expanded by a factor of 2. (bottom) The 15-yr running mean $T_a - T_o$ during DJF estimated as described in the text. The vertical dashed line shows the time when $T_a - T_o$ reaches the threshold that bifurcates the importance of the ENSO nonlinearity.

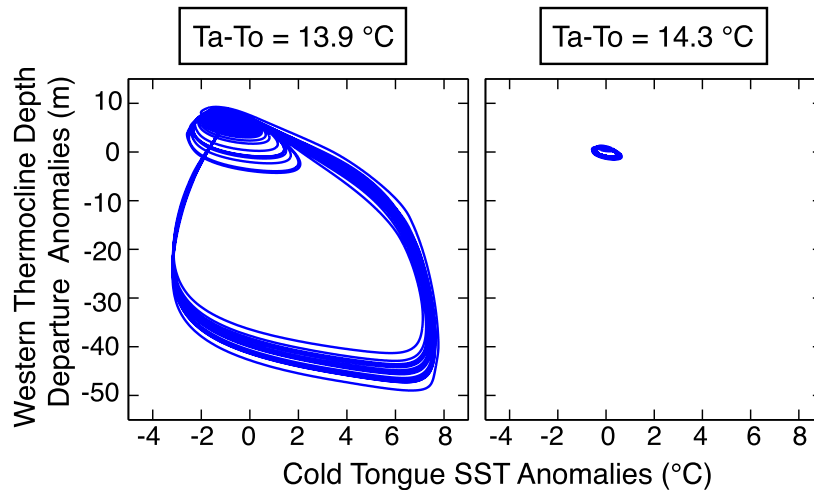
than the ocean interior beneath the thermocline because of the large oceanic heat capacity and the slow oceanic circulation compared to the atmospheric counterparts. Therefore, as a transient response to global warming, $T_a - T_o$ should become larger as Earth warms, and this may be why no NDH and EENs are detected in a warmer climate in GFDL-ESM2M. To test this hypothesis, we have calculated the time series of $T_a - T_o$ in GFDL-ESM2M using the warm pool SST as a proxy for T_a (because, in section 3, T_a is equal to the radiative–convective equilibrium temperature) and the temperature 100 m below the thermocline, averaged over the cold tongue region (5°S – 5°N , 120° – 90°W), as a proxy for T_o (see also section 2). For reference, the typical thermocline depth for this region is about 50 m.

Figure 5 shows the time series of MPI, the cold tongue SST, NDH, and $T_a - T_o$ for the piControl, RCP8.5, and abrupt4xCO2 runs of GFDL-ESM2M. As already pointed out in Fig. 2, GFDL-ESM2M occasionally exhibits EENs and NDH in piControl (nonlinear regime) but no EENs and NDH in abrupt4xCO2 (linear regime).

In accordance with a gradual warming in RCP8.5, the model exhibits a clear transition from the nonlinear regime to the linear regime. More importantly, our key parameter $T_a - T_o$ also increases by about 1°C as the regime shifts, suggesting that the ideas obtained from the idealized model experiments are consistent with the behavior of GFDL-ESM2M.

To further confirm the consistency between the idealized model and GFDL-ESM2M, in Fig. 6, we have also plotted phase diagrams showing the relationship between the cold tongue SST anomalies and western thermocline depth departure anomalies. The phase diagrams of both models exhibit a reasonable resemblance with each other, and the mechanism can be explained as follows. In the nonlinear regime with low upwelling efficiency, the Sverdrup transport caused by the trade wind recharges the heat in the equatorial mixed layer and the thermocline depth gradually becomes deeper than the norm, which in turn causes inefficient upwelling and, finally, an extremely warm SST anomaly in the cold tongue (i.e., EEN). In the linear regime with high upwelling efficiency, however, the trade wind cannot

a) Idealized Model



b) GFDL-ESM2M

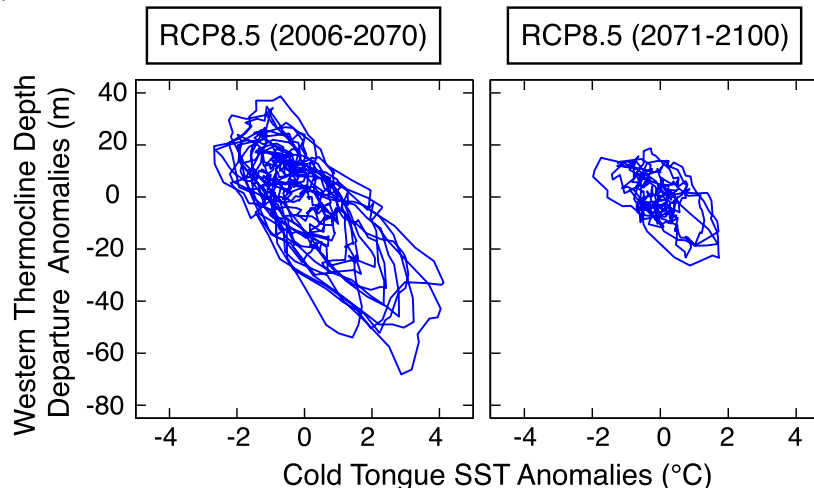


FIG. 6. (a) Phase diagrams showing the relationship between the cold tongue SST T_2 anomalies and the western thermocline depth departure h_1 anomalies simulated by the idealized model. The left (right) panel in (a) shows $T_a - T_o$ below (above) the threshold that bifurcates the importance of the ENSO nonlinearity. The point (T_2^*, h_1^*) circles clockwise as the model is integrated forward in time. (b) As in (a), but for GFDL-ESM2M under RCP8.5. The western thermocline depth is defined as the depth at which the vertical temperature gradient reaches its maximum and is averaged over 5°S – 5°N , 140°E – 150°W . After removing monthly climatology and centennial linear trends, a 3-month running mean is applied.

recharge the heat in the mixed layer because of the stronger upwelling cooling, so the thermocline cannot become deep enough to excite an event with a huge SST anomaly in the east.

4. Nonlinear ENSO warming suppression (NEWS) causing a La Niña-like mean-state response to global warming

In this section, we further compare the idealized model with observations and GFDL-ESM2M output to

show that the forced, nonlinear EEN dissipation due to the transient increase of $T_a - T_o$ has a warming suppression effect on the mean state of the eastern equatorial Pacific SST. We also explore some necessary conditions to simulate this mechanism by comparing GFDL-ESM2M to other models. Furthermore, we focus on the different mean-state responses between gradual and abrupt warming runs to emphasize the transient aspect of this mechanism and to determine the direction of causality between the ENSO amplitude change and the mean-state change.

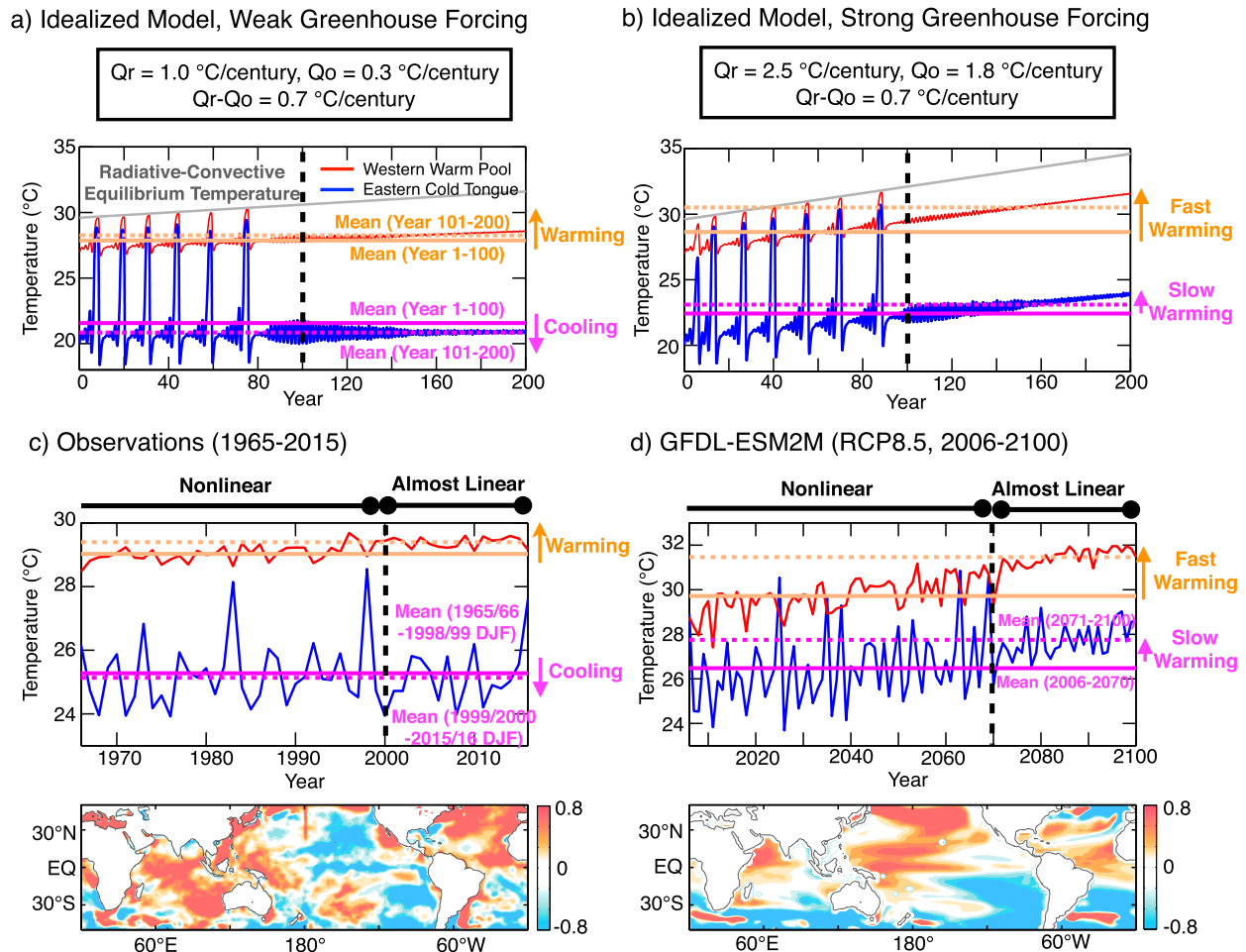


FIG. 7. (a) As in Fig. 4b, but with the mean SST over the years before (colored solid) and after (colored dashed) the time when the ENSO nonlinearity becomes unimportant (black dashed). Orange (magenta) lines show the mean SST of the western warm pool (eastern cold tongue) SST. Also shown is the prescribed radiative–convective equilibrium temperature (gray). (b) As in (a), but for stronger greenhouse forcing with $T_a - T_o$ kept the same as in (a). (c) As in (a), but for observations during DJF. Bottom panel of (c) is the map of the annual-mean observed SST trends ($^{\circ}\text{C century}^{-1}$) during 1965–2015 computed relative to the tropical Pacific mean trends (30°S – 30°N , 90°E – 60°W). Blue color denotes a warming slower than the tropical Pacific mean, not necessarily a cooling. (d) As in (c), but for GFDL-ESM2M under RCP8.5.

a. NEWS as a forced response to global warming

In the previous section, we have shown that El Niño events cannot become huge in a warming climate in GFDL-ESM2M because the transient heating rate difference between the atmospheric and oceanic reservoirs enhances the cooling effect of the mean upwelling, which in turn damps the NDH necessary to produce a large positive eastern equatorial SST anomaly. In the introduction, we reviewed AJ04’s observational evidence that NDH causes the El Niño–La Niña amplitude asymmetry and that the NDH warming effect is comparable to LDH only for EENs. Therefore, because of the NDH dissipation, if El Niño events are weakened but La Niña events remains almost unchanged, then we expect a nonlinear rectification effect

on the climatological mean state (Battisti and Hirst 1989; Jin et al. 2003), which causes a La Niña-like mean-state SST response to global warming.

Figures 7a,b show the results of the idealized model runs with weak and strong greenhouse forcing. We use the parameters of $Q_r = 1.0^{\circ}\text{C century}^{-1}$ and $Q_o = 0.3^{\circ}\text{C century}^{-1}$ for the weak greenhouse forcing run (identical to Fig. 4b) and $Q_r = 2.5^{\circ}\text{C century}^{-1}$ and $Q_o = 1.8^{\circ}\text{C century}^{-1}$ for the strong greenhouse forcing run. For both runs, we kept $Q_r - Q_o$ (therefore $T_a - T_o$) the same, $0.7^{\circ}\text{C century}^{-1}$, but only changed the magnitude of warming. As discussed in the last section, the key parameter for the importance of NDH is $T_a - T_o$, rather than T_a or T_o individually, so the nonlinear behaviors are reasonably similar between the two runs except for minor differences due to the chaotic nature of the dynamical system.

In both experiments, the warm pool SST (i.e., the MPI) warms with a strict upper bound of the radiative–convective equilibrium temperature. Comparing the first century (nonlinear regime) with the second century (linear regime), the mean-climate warm pool SST warms accordingly. On the other hand, because of the EEN cessation at about year 100 (i.e., $T_a - T_o = 14.2^\circ\text{C}$), the mean-state cold tongue SST experiences cooling (weak greenhouse forcing) or slow warming (strong greenhouse forcing) during the two centuries. In particular, it is interesting that global warming forcing by itself can even cool the eastern equatorial Pacific, if the forcing is not too strong. Of course, this cooling does not violate the second law of thermodynamics. The reason why the cold tongue SST cools is simply because the upwelling of the cool water is no longer interrupted by EENs in a warmer climate. We believe this cooling is hard to be realized solely by the ocean dynamical thermostat (Clement et al. 1996) because both the radiative–convective equilibrium temperature and the upwelling water temperature, in this particular experiment, are designed to warm. Then, the strong greenhouse forcing run clearly shows that, even if the EEN dissipation cooling effect is much weaker compared to the radiative warming, the EEN effect is still detectable in the form of zonal difference of the warming rate.

In summary, the warm pool SST is almost solely bounded by the radiative convective equilibrium temperature change, but the cold tongue SST is controlled by two competing effects: the radiative warming and the EEN-dissipation cooling. Therefore, at least in this idealized model, the western equatorial Pacific warms faster than the east as a result of a forced response to global warming. We have hypothesized that this mechanism may be the cause of the La Niña-like mean-state warming in GFDL-ESM2M and possibly cause part of the observed trend during the satellite era. We hereafter refer to this mechanism as NEWS and will further explore whether it is actually realistic. The essential physics of the NEWS mechanism is that the increasing $T_a - T_o$, because of the transient heating rate difference between the atmospheric and oceanic reservoir, dissipates EENs as a result of the enhanced upwelling efficiency, and then, as suggested by Jin et al. (2003), the weakened nonlinear ENSO amplitude causes a rectification cooling effect on the climatological-mean cold tongue SST.

The top panel of Fig. 7c shows the warm pool and cold tongue SST observed during DJF from 1965/66 through 2015/16. As we have already seen in Fig. 3, the nonlinear regime continued toward the end of the past century, and since then it has been almost linear. At least by this metric, the warm pool is warming much faster than the

cold tongue (where the SST has slightly cooled), which is consistent with the NEWS mechanism. Though this mean cooling is undoubtedly exaggerated by natural variability, our point here is that, even if the cold tongue has been cooling during the past half a century, part of this trend in the tropical Pacific may be forced by global warming, as shown in Fig. 7a. Because of the zonal difference of the warming rate, the spatial pattern of the SST trend looks like a La Niña-like warming (Fig. 7c, bottom panel).

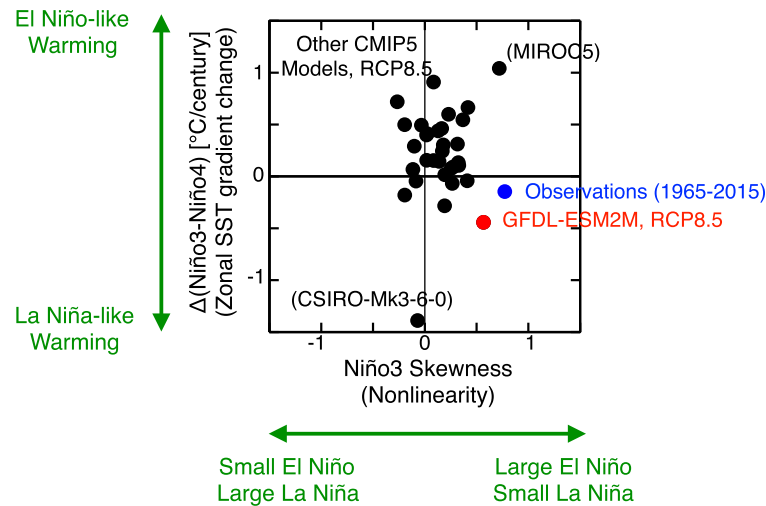
GFDL-ESM2M is also consistent with NEWS. Figure 7d shows the modeled warm pool and cold tongue SST during DJF in RCP8.5. As we have seen in Fig. 5, the nonlinear regime appears to end in about 2070. This run looks more similar to the strong greenhouse forcing experiment in the idealized model (Fig. 7b). Because of the strong greenhouse forcing, one might have the impression that the NEWS effect appears to be subtle in the time series (Fig. 7d, top panel). The spatial pattern of the trend (Fig. 7d, bottom panel), however, undoubtedly shows that the western Pacific warms faster than the east, which is consistent with the NEWS mechanism.

b. Necessary conditions of NEWS

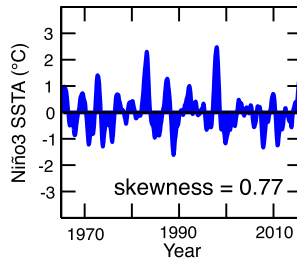
We expect that the atmospheric heating should be faster than the oceanic heating in most CMIP5 models, not only GFDL-ESM2M. Why, then, do the majority of the CMIP5 models lack the La Niña-like trend associated with NEWS? As shown in the idealized model experiments, the nonlinear dynamics of ENSO is an essential ingredient of NEWS. If GCMs do not capture realistic nonlinear ENSO dynamics, the NEWS mechanism cannot operate, which could have implications for the reliability (or lack thereof) of tropical mean climate change projections by those models.

Figure 8a (and Table 1) shows the relationship between the ENSO nonlinearity and the zonal SST gradient response to warming calculated for 32 CMIP5 models and observations. Here, the ENSO nonlinearity is defined as the skewness of detrended 11-month running mean SST anomalies and is averaged over the Niño-3 region so that positive skewness means larger El Niños and smaller La Niñas. The zonal SST gradient is defined as Niño-3 SST anomalies minus Niño-4 (5°S – 5°N , 160°E – 150°W) SST anomalies as in KHB17 so that a positive $\Delta(\text{Niño-3} - \text{Niño-4})$ means an El Niño-like mean-state warming. Interestingly, the majority of the models exhibit little nonlinearity of ENSO and large El Niño-like warming trends, but observations and GFDL-ESM2M both show large nonlinearity and La Niña-like warming trends. Therefore, it is possible that only GFDL-ESM2M can capture the Pacific SST

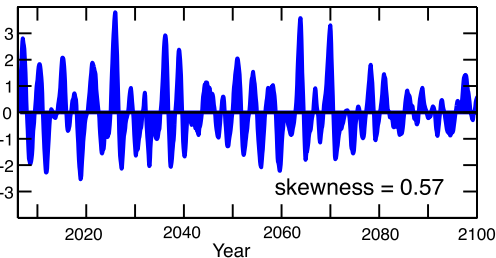
a) Zonal SST gradient change and Nonlinearity of the CMIP5 models



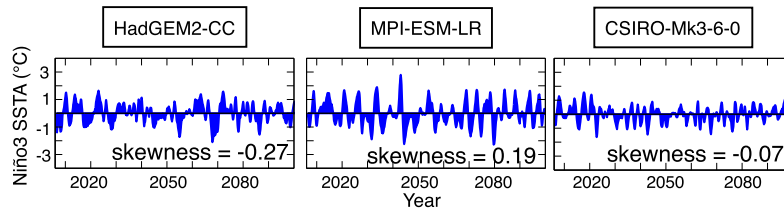
b) Observations



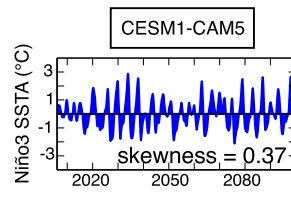
c) GFDL-ESM2M



d) Opposite / Insufficient asymmetry



e) Few extreme El Niños



f) Excessive extreme El Niños

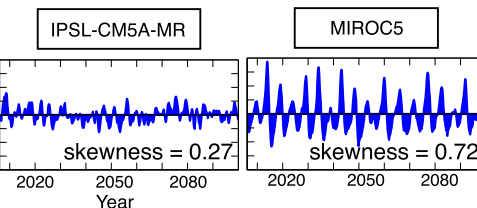


FIG. 8. (a) Scatterplot showing the relationship between the ENSO nonlinearity (defined as the skewness of detrended 11-month running mean Niño-3 index) and the zonal SST gradient change (defined as the centennial linear trend of Niño-3 minus Niño-4) under RCP8.5, calculated for GFDL-ESM2M (red) and 31 CMIP5 models (black). Also shown is the value for observations during 1965–2015 (blue), which should not be directly compared to the projections under RCP8.5. (b) Detrended Niño-3 SST anomaly (SSTA) for observations. An 11-month running mean is applied. (c) As in (b), but for GFDL-ESM2M under RCP8.5. (d) As in (c), but for CMIP5 models with negative or small skewness. (e) As in (d), but with few extreme El Niño events. (f) As in (d), but with excessive extreme El Niño events. Model data is from the PCMDI website.

TABLE 1. Table showing the numerical values ($^{\circ}\text{C century}^{-1}$) shown in Fig. 8a. The GFDL-ESM2M values are highlighted in boldface font. The values obtained from observations during 1965–2015 are 0.77° and $-0.15^{\circ}\text{C century}^{-1}$ for the Niño-3 skewness and $\Delta(\text{Niño-3} - \text{Niño-4})$, respectively. (Acronym expansions are available online at <http://www.ametsoc.org/PubsAcronymList>.)

Model	Niño-3 skewness	$\Delta(\text{Niño-3} - \text{Niño-4})$	Model	Niño-3 skewness	$\Delta(\text{Niño-3} - \text{Niño-4})$
ACCESS1.0	0.16	0.46	GISS-E2-H	0.13	0.44
ACCESS1.3	-0.11	0.07	GISS-E2-R	-0.19	0.50
BCC_CSM1.1(m)	0.08	0.15	HadGEM2-CC	-0.27	0.72
BCC_CSM1.1	0.02	0.16	HadGEM2-ES	0.02	0.40
BNU-ESM	0.19	-0.28	INM-CM4.0	0.02	0.41
CanESM2	-0.10	0.29	IPSL-CM5A-LR	0.27	0.09
CCSM4	0.18	0.30	IPSL-CM5A-MR	0.27	-0.07
CESM1(BGC)	0.32	0.31	IPSL-CM5B-LR	0.09	0.91
CESM1(CAM5)	0.37	0.55	MIROC5	0.72	1.04
CNRM-CM5	0.17	0.24	MIROC-ESM-CHEM	0.33	0.11
CSIRO Mk3.6.0	-0.07	-1.39	MIROC-ESM	0.32	0.13
FGOALS-g2	-0.03	0.49	MPI-ESM-LR	0.19	0.02
FIO-ESM	-0.19	-0.18	MPI-ESM-MR	0.25	0.08
GFDL CM3	-0.09	-0.04	MRI-CGCM	0.14	0.15
GFDL-ESM2G	0.41	-0.04	NorESM1-ME	0.42	0.66
GFDL-ESM2M	0.57	-0.44	NorESM1-M	0.23	0.60

response to warming in the real world. The larger zonal SST gradient change in GFDL-ESM2M (RCP8.5) than in observations (1965–2015) could partly be explained by the greenhouse warming strength, but it could also be attributed to the ENSO amplitude bias of GFDL-ESM2M (Figs. 8b,c).

Figures 8d–f show some examples of detrended 11-month running mean Niño-3 time series from the CMIP5 models. Figure 8d shows three models, HadGEM2-CC, MPI-ESM-LR, and CSIRO Mk3.6.0, which exhibit opposite or insufficient ENSO asymmetry compared to observations. CSIRO Mk3.6.0 has a strong warming near the Niño-4 region, and therefore it

exhibits an extremely negative $\Delta(\text{Niño-3} - \text{Niño-4})$ (Fig. 8a). Nevertheless, the spatial pattern looks more like the multimodel mean El Niño-like pattern (not shown; qualitatively similar to the right panel of Fig. 9b). Figure 8e shows two models, CESM1(CAM5) and IPSL-CM5A-MR, which exhibit better asymmetry. These models, however, do not have EENs that stand out among other El Niño events, which are also essential for the NEWS mechanism to work. An interesting outlier is MIROC5, shown in Fig. 8f. This model is the only model that exhibits more realistic skewness than GFDL-ESM2M (Fig. 8a), but it also exhibits the largest positive $\Delta(\text{Niño-3} - \text{Niño-4})$, or a strong El Niño-like

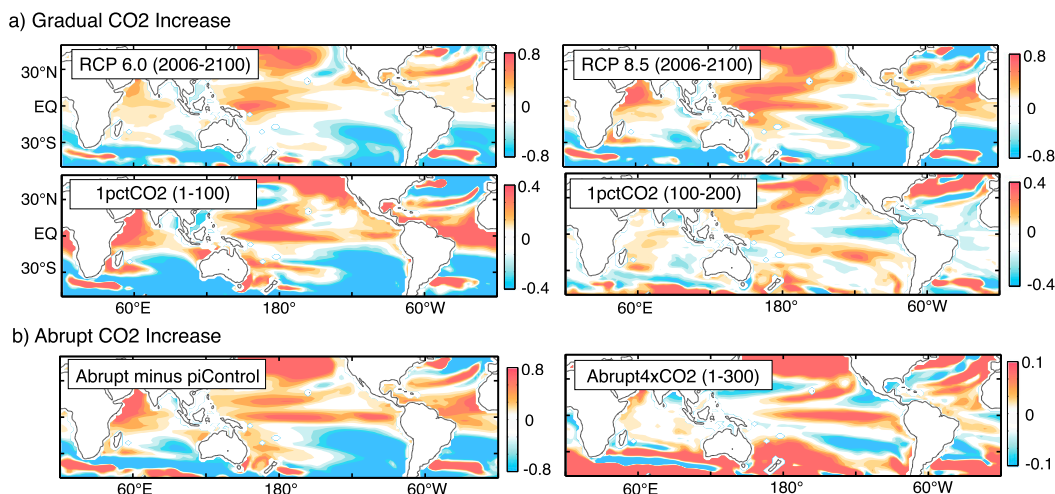


FIG. 9. (a) As in the bottom panel in Fig. 7d, but for RCP6.0, RCP8.5, and the first and second halves of the 1pctCO2 run. (b) Left panel shows the warming response calculated as difference of SST climatology ($^{\circ}\text{C}$) in the manner of abrupt4xCO2 (years 101–300) minus piControl. Right panel of (b) as in (a), but for abrupt4xCO2 (years 1–300) ($^{\circ}\text{C century}^{-1}$).

warming. The time series shows a large number of EENs, so it is possible that NDH in this model may be too large, more like the top-left panel of Fig. 4a with small climatological $T_a - T_o$. Thus, it may be hard for $T_a - T_o$ to surpass the threshold at which the importance of ENSO nonlinearity bifurcates. Further investigation is needed to understand why MIROC5 does not simulate NEWS despite its realistic nonlinearity.

c. Transient feature of NEWS and the direction of causality between the ENSO amplitude change and the mean-state trends

Though we have used piControl and abrupt4xCO2 to show the EEN dissipation in the previous section, the rectification effect on the mean-state SST exhibits some important differences between a gradual CO₂ increase and an abrupt one. Figures 9a,b show the spatial pattern of the SST trend relative to the Pacific mean trend for gradual and abrupt CO₂ increases. As we have discussed so far, the mean-state SST responses in the gradual CO₂ runs are clearly La Niña-like, which we believe are associated with NEWS. The warming response of the abrupt runs (expressed as abrupt4xCO2 minus piControl), however, exhibits more zonally uniform warming. If we look at this pattern carefully, the western Pacific exhibits a reasonably similar spatial structure to the gradual runs, but it also exhibits additional warming anomalies in the east.

The 300-yr trends calculated for abrupt4xCO2 might reveal the cause of its different behavior (Fig. 9b, right panel). The spatial structure of this trend pattern looks quite similar to the multimodel mean calculated for CMIP5 (Ying et al. 2016; Zheng et al. 2016). Given that this multimodel-mean El Niño-like pattern is associated with the slow response of the Walker circulation change (Held and Soden 2006; Vecchi and Soden 2007; Held et al. 2010) or the ocean dynamics (Luo et al. 2015, 2017), the spatial pattern of the “abrupt4xCO2 minus piControl” could be interpreted as the superposition of the slow El Niño-like pattern and the transient La Niña-like pattern associated with NEWS. This idea of superposition is consistent with the fact that the trends shown in the second century of the 1pctCO2 run are overall weaker than those shown in the first century because the NEWS mechanism is slow but transient and that the trend pattern calculated for the full two centuries in 1pctCO2 does not look too different from the abrupt4xCO2 minus piControl (not shown).

The transient feature of NEWS is schematically shown in Fig. 10. If we transiently warm the atmosphere faster than the ocean, the resulting temperature difference would tend to enhance the climatological upwelling efficiency, which annihilates EENs. As we have

repeatedly explained, this contrast between a normal climate (Fig. 10a) and a transiently warming climate (Fig. 10b) is the basis of the NEWS mechanism. Once the system reaches its equilibrium, however, the oceanic temperature increase catches up with that of the atmosphere, which may eventually establish EENs again (Fig. 10c). Therefore, the NEWS effect is not necessarily expected to continue perpetually in an equilibrated warmer climate. This renewal of EENs, however, cannot be detected under abrupt4xCO2 as shown in Fig. 5, which may be partly because the 200-yr time span might be too short for the oceanic reservoir temperature to catch up with the radiative–convective surface temperature.

We have to remember, however, that the CO₂ increase in the real world should be gradual, not abrupt. Therefore, at least based on these results from GFDL-ESM2M, the realistic SST warming pattern during this century should be closer to the La Niña-like one associated with the transient NEWS mechanism. Some previous studies (e.g., Held et al. 2010) have shown that the La Niña-like fast response to abrupt CO₂ forcing might be due to the ocean dynamical thermostat (Clement et al. 1996). The response time scale of the ocean dynamical thermostat, however, is too short to appear in the centennial trend of the gradual warming runs because the shallow oceanic overturning circulation that largely controls the thermostat mechanism takes only about a couple of decades at the longest to complete its full circuit and to reach quasi equilibrium. This time scale is clearly different from the ENSO response to global warming, which takes almost a full century for multiple EENs to dissipate and for the NEWS effect to emerge.

The different response between the gradual and abrupt runs could also help elucidate the direction of causality between the EEN dissipation and the mean-state SST change. As we have shown, in the abrupt4xCO2 run, the mean-state warming response is zonally uniform because the slow El Niño-like response also contributes to the total trend. Interestingly, however, the ENSO amplitude still keeps its weakened amplitude, without any EENs, even in the late third century (Fig. 5). This weakened amplitude means that the nonlinear ENSO amplitude is not affected by the zonally uniform mean-state change in the abrupt run, though we see a hint of increased LDH (Fig. 2). Therefore, at least in GFDL-ESM2M, the weakened nonlinear ENSO amplitude is more likely to be a cause, rather than an effect, of the La Niña-like mean-state change in the gradual CO₂ increase runs. This result questions the views presented in some earlier studies that treated ENSO as more like a linear mode (e.g., Timmermann et al. 1999;

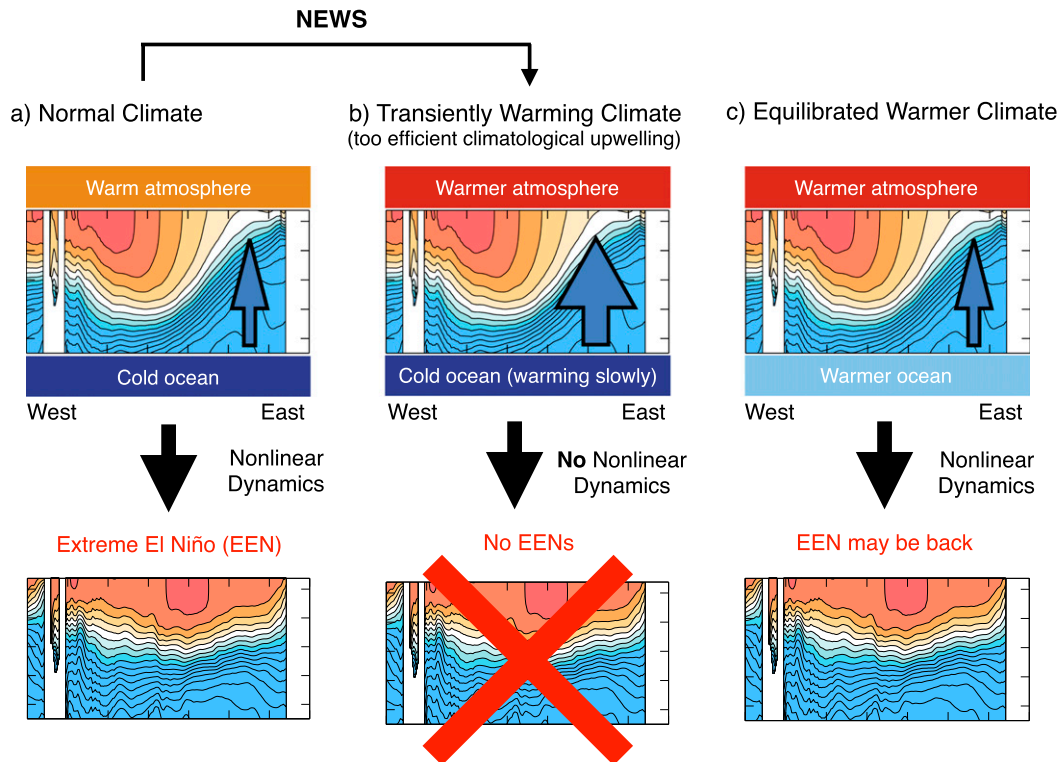


FIG. 10. (a) Schematic showing the relationship between $T_a - T_o$ and the nonlinear ENSO dynamics in a normal climate. The blue arrow shows the efficiency of climatological upwelling. Contours show the meridional-mean equatorial potential temperature of the upper Pacific Ocean (0–200 m). (b) As in (a), but for a transiently warming climate. (c) As in (a), but for an equilibrated warmer climate.

An and Jin 2000; Fedorov and Philander 2000; Urban et al. 2000; Wang and An 2001, 2002) but is consistent with work by Atwood et al. (2017) where they took nonlinearity into account. We believe, however, that this argument remains to be too speculative and insufficient to demonstrate causality. Closer investigation is needed to further verify the causality.

d. The Pacific mean-state climate change as a forced response to global warming

Figure 11 presents three warming scenarios that can be simulated by state-of-the-art GCMs. Figure 11a shows the NEWS scenario, where gradual global warming increases $T_a - T_o$ and triggers the transient NEWS mechanism to yield a La Niña-like trend (Fig. 9a). To the best of our knowledge, this scenario is only simulated by GFDL-ESM2M, which exhibits the second-most realistic ENSO nonlinearity among the 32 CMIP5 models investigated here. As shown by KHB17 in their Fig. 3, the La Niña-like trend then strengthens the Walker circulation, whose structure is remarkably similar to the observed trend during the satellite era. Because the NEWS effect is so strong, GFDL-ESM2M does not use the Walker circulation for weakening the

global-mean atmospheric circulations to sustain the energy and water balance (Held and Soden 2006), as the majority of GCMs do (Vecchi and Soden 2007). KHB17 also showed that the strengthening Walker circulation in GFDL-ESM2M is still consistent with the global mean energy–water balance (Held and Soden 2006). On the other hand, the reason why the majority of the CMIP5 models do not simulate NEWS appears to be that the ENSO nonlinearity of these models is unrealistic (Figs. 8 and 11b).

Figure 11c shows the abrupt warming scenario, where CO_2 is abruptly increased instantaneously. Even for the abrupt increase, the increase of $T_a - T_o$ dissipates EENs as shown in Fig. 2, so the NEWS mechanism is expected to work. The mean-state SST rectification effect of NEWS, however, appears to be masked by other mechanisms as follows. First, because of the short time span of the CO_2 increase, the effect of the ocean dynamical thermostat (Clement et al. 1996) might dominate the fast SST response as suggested by Held et al. (2010). Moreover, once the system reaches its quasi equilibrium, the energy–water balance eventually starts to weaken the Walker circulation as a slow response, which helps an El Niño-like trend emerge (Fig. 9b, right

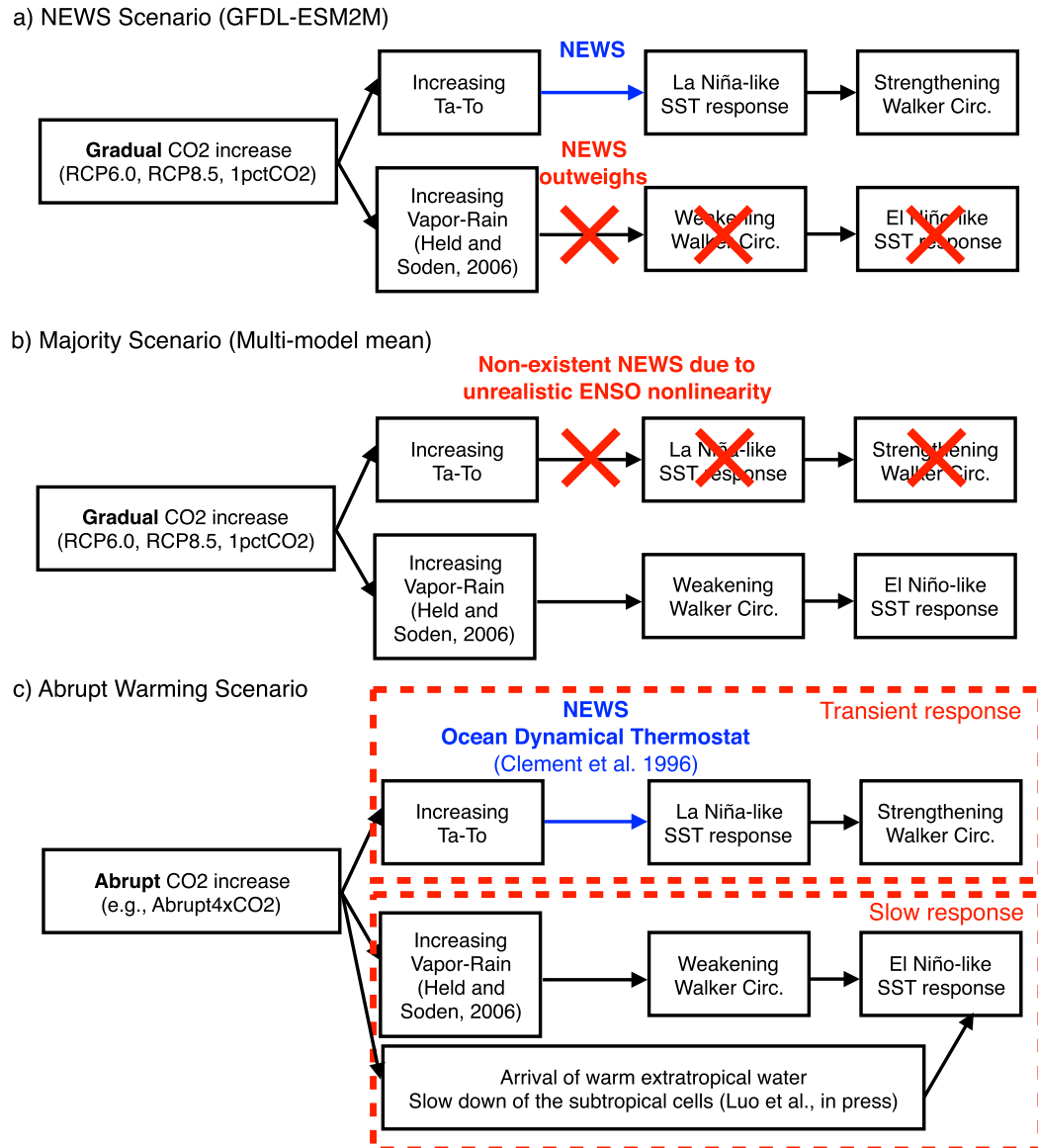


FIG. 11. (a) Flowchart showing the scenario where the NEWS mechanism works, which appears to be realized only by GFDL-ESM2M with a gradual increase of CO_2 . (b) As in (a), but without NEWS. The majority of the CMIP5 models follows this scenario. (c) As in (a), but for an abrupt warming scenario.

panel). It is also possible that the ocean dynamics could also contribute to the El Niño-like trend, as recently shown by Luo et al. (2015, 2017). Therefore, by subtracting the piControl climatology from the equilibrated abrupt4x CO_2 climatology, we detect a superposition of the La Niña-like trend caused by the transient mechanisms and the El Niño-like trend caused by the energy-water balance, which is a more zonally uniform SST warming (Fig. 9b). Despite the zonally uniform mean-state SST change, the nonlinear part of the ENSO amplitude is kept suppressed in a warmer climate (Fig. 2). Therefore, though our explanation remains speculative,

we believe it is more likely that the weakening ENSO amplitude under gradual warming is a cause, rather than an effect, of the mean-state SST change.

5. Implications for multidecadal natural variability of the Pacific SST and global warming hiatuses

Because the NEWS mechanism is driven by the reservoir temperature difference between the atmosphere and ocean, the root cause of this difference does not have to be greenhouse forcing, as long as Earth is transiently heated and the lower atmosphere warms faster

than the oceanic interior. Therefore, even if Earth is warmed by natural variability, rather than an anthropogenic forcing, the NEWS mechanism should still operate. The opposite mechanism might also work if Earth is cooled by a certain cause. In this section, we further explore the idealized model and the piControl run to investigate some implications of NEWS for multidecadal natural variability of the Pacific SST. We then discuss the effect of this natural variability on global warming.

a. IPO-like natural multidecadal variability explained by the NEWS–NECS cycle

If Earth's atmosphere were cooled by a random natural cause, this cooling would transiently decrease $T_a - T_o$, making upwelling less efficient and producing more EENs with nonlinear ENSO dynamics. The increased number of EENs must then have a rectification warming effect on the mean-state cold tongue SST, producing an El Niño-like mean climate. If the NEWS mechanism is realistic, this opposite mechanism should also operate. Hereafter, we refer to this mechanism as the nonlinear ENSO cooling suppression (NECS).

Moreover, as Kosaka and Xie (2013) and many others have discussed in relation to the recent global warming slowdown, it is known that a prolonged La Niña-like mean state cools the atmospheric temperature, and vice versa. Therefore, we expect that the effect of NEWS (NECS) can eventually cause NECS (NEWS), and the repetition of NEWS and NECS might contribute to multidecadal natural variability. The idea can be summarized into five steps as follows:

- 1) When the atmosphere is warmed, the NEWS mechanism yields a La Niña-like Pacific mean climate.
- 2) The prolonged La Niña-like Pacific mean climate eventually cools the atmosphere.
- 3) When the atmosphere is cooled, the NECS mechanism yields an El Niño-like Pacific mean climate.
- 4) The prolonged El Niño-like Pacific mean climate eventually warms the atmosphere.
- 5) Repeat steps 1–4.

Based on this idea, we have further generalized the idealized model by making the atmospheric reservoir temperature sensitive to the cold tongue SST as described in section 2. In this model, the atmosphere also has its normal mode of natural variability that restores the atmosphere toward the radiative–convective equilibrium temperature and is forced by the cold tongue SST. Figure 12a shows the warm pool and cold tongue SST simulated by the idealized model. Because of the forced oscillation of the atmospheric reservoir temperature, $T_a - T_o$ exhibits a sinusoidal variation so that it

crosses the threshold that bifurcates the importance of the ENSO nonlinearity (i.e., $T_a - T_o = 14.2^\circ\text{C}$). Therefore, during a nonlinear ENSO phase, EENs emerge and suppress the cooling rate of the atmosphere by the cold tongue. The resulting warming pushes the system toward a linear ENSO phase by the NEWS mechanism. On the other hand, during a linear ENSO phase, EENs dissipate, and the cold tongue enhances the cooling rate of the atmosphere. The resulting cooling pushes the system toward a nonlinear ENSO phase by the NECS mechanism. This NEWS–NECS cycle exhibits a clear multidecadal oscillation that is reasonably similar to the interdecadal Pacific oscillation (IPO) observed in the real world.

Next, it would be interesting to investigate if GFDL-ESM2M reproduces this NEWS–NECS cycle. By taking a careful look at the piControl run shown in Fig. 5, one finds that NDH and EENs are weakened during about year 300 ± 50 . Therefore, we hypothesize that this amplitude variation might be understood in the context of the NEWS–NECS cycle. Figures 12b and 12c show the warm pool and cold tongue SST ($T_a - T_o$) and the SST trend pattern during years 211–400, respectively. During the first half of this period (Fig. 12b), $T_a - T_o$ has a clear positive trend, EENs dissipate in about year 260, and the Pacific SST exhibits a La Niña-like trend. Therefore, the first half of the period is consistent with the NEWS mechanism as described in the previous section. On the other hand, during years 306–400 (Fig. 12c), a negative trend of $T_a - T_o$, an increasing number of EENs, and an El Niño-like trend are detected, which is consistent with the NECS mechanism.

Because the normal mode frequency of the atmospheric natural variability ω and the sensitivity of atmospheric heating rate to the cold tongue SST γ are free parameters that are difficult to estimate based on currently available observational records, the aforementioned mechanism remains speculative in the sense that we have arranged the system to cross the $T_a - T_o$ threshold for producing realistic decadal variability. A more rigorous heat budget analysis is also needed to confirm that the natural $T_a - T_o$ variation in GFDL-ESM2M is induced by the modulation of heating by the Pacific mean-state SST variations. Nevertheless, the mechanism makes physical sense, so it is expected to contribute to the observed IPO-like multidecadal SST variability at least to some extent. The remarkable resemblance between the idealized model and GFDL-ESM2M also increases the interest in investigating this NEWS–NECS hypothesis further as one of many possible mechanisms of low-frequency natural SST variability, such as the IPO. It is also consistent with previous studies that suggested that the

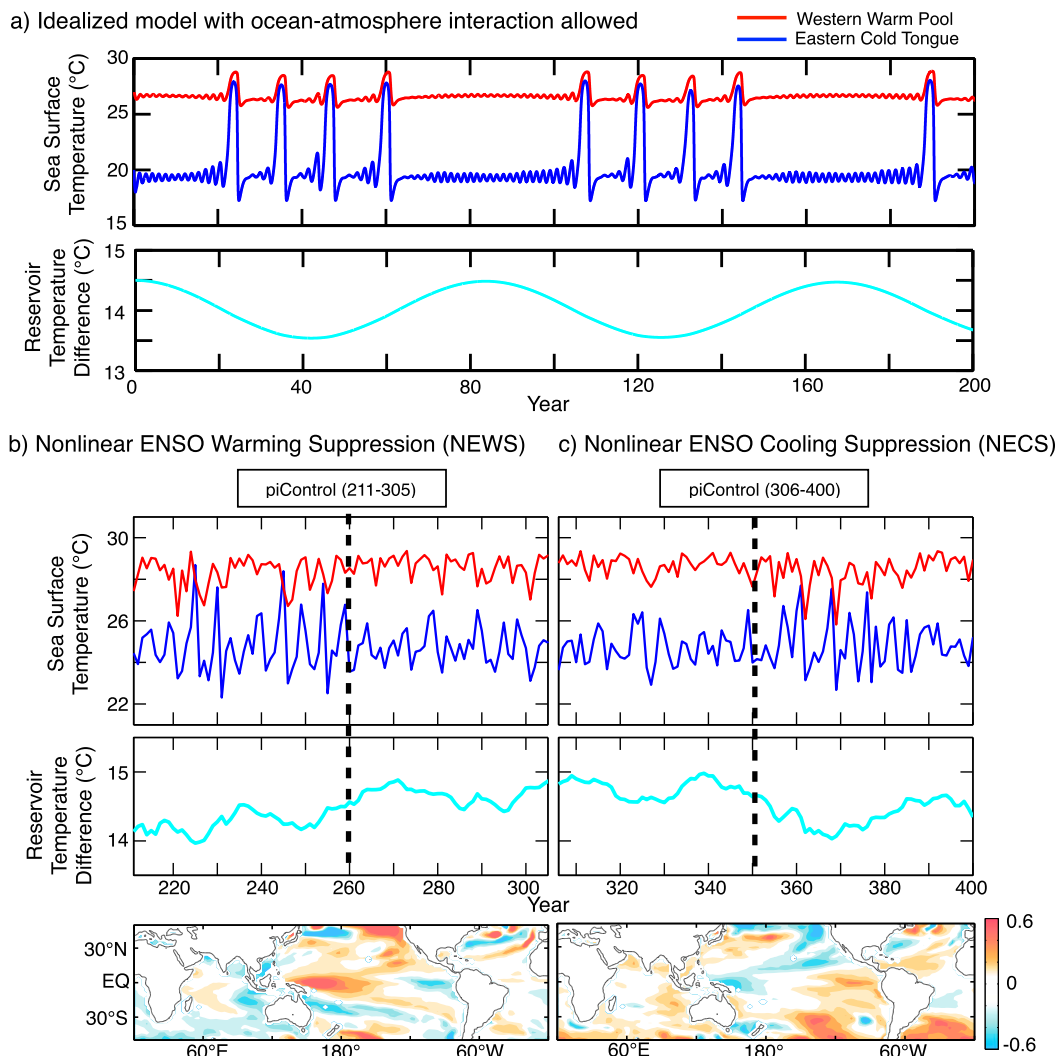


FIG. 12. (a) Top panel as in Fig. 4a, but the atmospheric reservoir is not fixed to the radiative–convective equilibrium temperature. Bottom panel of (a) is $T_a - T_o$. (b) Top and middle panels as in (a), but for GFDL-ESM2M under piControl (years 211–305 for DJF). A 15-yr running mean is applied to $T_a - T_o$. The bottom panel of (b) as in the bottom panel of Fig. 7d, but for piControl (years 211–305). (c) As in (b), but for years 306–400.

ENSO nonlinearity and/or EENs may play a role in rectifying the mean-state SST (e.g., An et al. 2005) or in changing the phase of the IPO (e.g., Meehl et al. 2016). Model-based process studies using GCMs and, if possible, observational verifications might shed new light on our understanding of the tropical Pacific multidecadal natural variability.

b. Implications for global warming hiatuses

The main idea presented by Kosaka and Xie (2013, 2016) was to explain the global warming hiatuses and slowdowns by prescribing the Pacific multidecadal SST variability. Therefore, if we hypothesize that the NEWS–NECS cycle explains part of the Pacific low-frequency natural SST variability, one straightforward

societal application of the NEWS–NECS cycle may be an attempt to explain global warming hiatuses. In this subsection, we further investigate global warming hiatuses using the idealized model and compare them to the observed global warming hiatuses.

Figure 13a shows the atmospheric natural variability simulated by the idealized model with zero sensitivity to the cold tongue SST. The heating rate of radiative–convective equilibrium temperature and oceanic reservoir temperature are chosen to be $Q_r = 2.0^\circ\text{C century}^{-1}$ and $Q_r = 1.9^\circ\text{C century}^{-1}$, respectively. The atmospheric reservoir temperature is strongly restored toward the prescribed, increasing radiative–convective equilibrium temperature that serves as an analog of greenhouse forcing. From this simulation, it is confirmed that, though

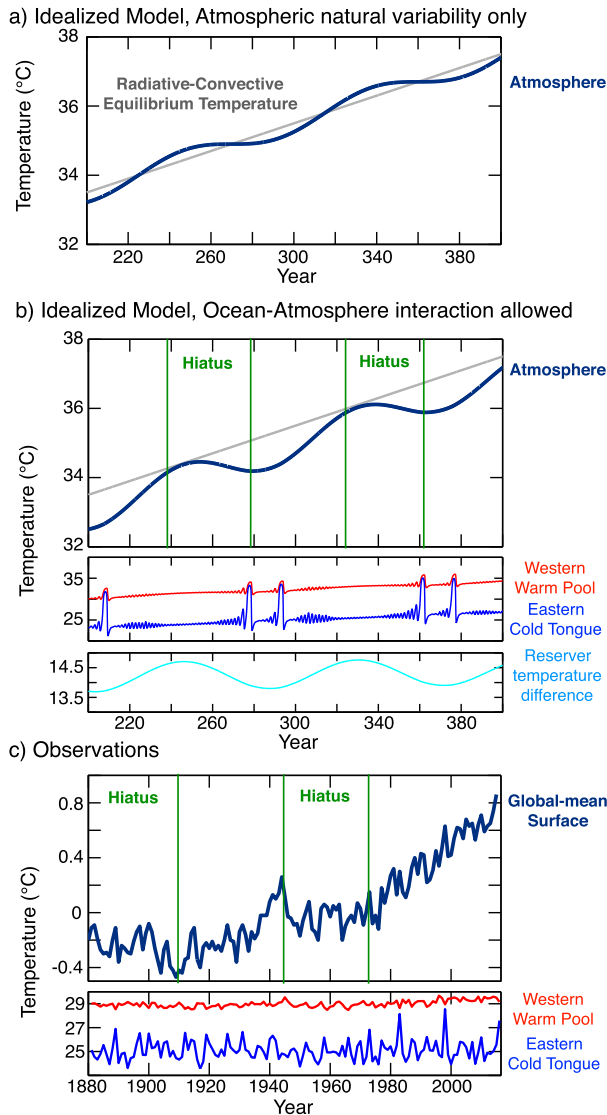


FIG. 13. (a) Atmospheric reservoir temperature simulated by the idealized model with zero atmospheric sensitivity to the cold tongue SST (navy blue line). Also shown is the prescribed radiative–convective equilibrium temperature (gray line). (b) Top panel as in (a), but for nonzero atmospheric sensitivity to the cold tongue SST. Also shown are the periods of global warming hiatuses (green lines). Middle and bottom panels of (b) as in Fig. 12a, but increasing the radiative–convective equilibrium temperature and oceanic reservoir temperature. (c) As in the top and middle panels of (b), but for observations. Atmospheric reservoir temperature is replaced by annual-mean, global-mean surface temperature relative to the base period of 1951–80. SST is averaged over DJF.

the atmospheric temperature exhibits weak oscillations and slowdowns, occasional negative decadal trends such as those observed in the real world are not simulated solely by the atmospheric natural variability under the parameter values and initial conditions used here.

Next, as described in section 2, we have allowed ocean–atmosphere interaction to operate in the idealized model. Figure 13b shows the result of this simulation. Because the atmosphere is sensitive to the cold tongue SST, the model exhibits well-defined hiatus periods where the atmospheric temperature does not experience a monotonic increase. It is consistent with the NEWS–NECS cycle that the warming trend of the atmospheric temperature is boosted by the emergence of EENs at the end of the hiatus periods and is moderated by the absence of EENs during the prolonged linear ENSO phase. As a feature of the forced oscillation, the frequency of the atmospheric variability is slightly modulated by the IPO-like multidecadal SST variability. For the ocean, on the other hand, relatively large variations of $T_a - T_o$ forced originally by the low-frequency variations of EENs, are in turn necessary to repeatedly cross the threshold temperature (i.e., $T_a - T_o = 14.2^\circ\text{C}$) to maintain the low-frequency variations of NDH and EENs. If this is the case, both atmospheric and oceanic roles regarding the NEWS–NECS cycle are important for amplifying the emergence and termination of multiple hiatus periods, instead of the atmosphere being unidirectionally forced by the “prescribed” SST multidecadal variability. In addition, considering that the key metric of the NEWS–NECS cycle is the ENSO nonlinearity, the lack of realistic ENSO nonlinearity may be one of many reasons why some GCMs have difficulty reproducing the global warming hiatuses, at least without prescribing observed SSTs (Kosaka and Xie 2013, 2016) or trade winds (Watanabe et al. 2014) in the eastern Pacific. On the other hand, it is also reported that other GCMs reproduces the most recent slowdown (Meehl et al. 2014; Liu et al. 2016). Therefore, it remains uncertain how much the NEWS–NECS cycle contributes to hiatuses and slowdowns in the real world.

Though the data quality of the observational datasets is limited before the middle of the past century, we have further attempted to compare this result to observations. Figure 13c shows the annual-mean, global-mean surface temperature time series in place of the atmospheric reservoir and SST (the warm pool and cold tongue SST) during DJF 1880–2015. Overall, the qualitative features are similar to the results simulated by the idealized model. Particularly similar is the feature that the EENs in 1982/83 and 1997/98 (and possibly 1972/73) appear to have boosted the global warming trend during the early satellite era, which is also consistent with previous studies suggesting a relationship between global warming hiatuses and IPO phase changes. Based on the idea of the NEWS–NECS

cycle, we also expect some EENs during about 1910–30, which were not as clearly observed as during the early satellite era. It is also possible, however, that the lack of EENs during 1910–30 is, in part, due to the relatively poor data quality during this period.

6. Conclusions

In this study, we have investigated observational data and model output from an idealized nonlinear recharge oscillator model and GCMs (with an emphasis on GFDL-ESM2M) to obtain the following conclusions.

- 1) A nonlinear theory shows that extreme El Niño (EEN) events may currently be becoming less frequent, and if global warming continues, EENs may not be observed at the end of this century. At least one GCM is consistent with this theory.

Some earlier studies that suggested an increase of the ENSO variance under global warming treated ENSO as a linear mode. This study, on the other hand, incorporates nonlinear ENSO dynamics and reconsiders future changes to ENSO. In our idealized model and GFDL-ESM2M (which has the second-most realistic ENSO nonlinearity of the 32 CMIP5 models investigated here), the ENSO amplitude weakens substantially in a warmer climate. Because of the transient heating rate difference between the atmospheric and oceanic reservoir, the upwelling efficiency tends to become enhanced under global warming. When the reservoir temperature difference (and therefore upwelling cooling efficiency) surpasses a certain threshold, the equatorial thermocline cannot recharge the heat enough to collapse the climatological mean state so that the nonlinear heating effect no longer works to yield EENs (Figs. 2–6).

When the system approaches the threshold, the idealized model and GFDL-ESM2M predict that EENs become less frequent (Figs. 4 and 5). Though we do not have enough observational evidence to verify this behavior, it is at least consistent with the available observational evidence that relatively large El Niño events were observed in 1972/73, 1982/83, 1997/98, and 2015/16, and thus the interval between events has increased from 10 to 15, and to 18 yr. Based on this idea, one might speculate that the next large El Niño event may perhaps occur around 2035/36, although other chaotic variability and forcings may work to the contrary. If global warming continues, the theory further predicts that ENSO becomes more linear and that EENs might not be observed at the end of this century.

- 2) A reasonable La Niña-like warming scenario can be envisioned using the NEWS mechanism as a forced response to global warming.

The forced weakening of ENSO amplitude has a rectifying cooling effect on the mean-state cold tongue SST (Fig. 7). Because of the nonlinear heating effect, the number of large El Niño events decreases while the number of La Niña events remains nearly constant. Therefore, the mean climate becomes La Niña-like. This nonlinear rectification effect by itself is essentially the same but opposite to the effect that Jin et al. (2003) showed for the strengthening ENSO amplitude and the warming cold tongue SST. The novelty of the NEWS mechanism is that the weakening ENSO can be explained as a forced response to global warming (see the first conclusion), which then yields the La Niña-like mean state by the nonlinear rectification effect.

- 3) NEWS is different from the ocean dynamical thermostat.

Some earlier studies at the end of the past century showed that the forced response should be La Niña-like because the climatological upwelling cooling effect will compensate the radiative warming in the east but not in the west (Cane et al. 1997). This mechanism is called the ocean dynamical thermostat (Clement et al. 1996). The mechanism is, however, now thought to be less likely to explain a centennial trend because the upwelling water in the cold tongue becomes warmer and reaches equilibrium after only a couple of decades, when the warmed extratropical surface water arrives in the equatorial thermocline through the upper-oceanic subtropical cell.

The NEWS mechanism is essentially different from the ocean dynamical thermostat. The NEWS mechanism involves nonlinear ENSO dynamics, whereas the ocean dynamical thermostat does not invoke ENSO at all. One important difference between them is the time scale of the La Niña-like warming. Because the NEWS mechanism takes time for multiple EENs to dissipate, it requires almost a full century to produce the mature La Niña-like trend (see also Fig. 2 in KHB17). The time scale of the ocean dynamical thermostat, however, is less than a couple of decades at the slowest.

- 4) The well-known El Niño-like mean-state warming is only a “majority decision” based on currently available GCMs, most of which exhibit unrealistic nonlinearity of the ENSO dynamics. A particularly important metric that needs urgent improvement in GCMs is the ENSO nonlinearity.

The majority of the CMIP5 models exhibit an El Niño-like mean-state warming. Therefore, the ENSO

research community widely believes that the warming response is more likely to be El Niño-like and that the La Niña-like trend during the satellite era is a manifestation of pure natural variability. We have shown here, however, that this could be only a majority decision by the GCMs with unrealistic ENSO nonlinearity (Fig. 8). To the best of our knowledge, only one state-of-the-art GCM, GFDL-ESM2M, simulates the La Niña-like warming by the NEWS mechanism. Nevertheless, based on the realistic ENSO nonlinearity of this model and the remarkable structural resemblance of the Walker circulation change to that of observations (Fig. 3 in KHB17), we believe this could be an equally realistic (or even more plausible) response to warming. Further investigation is needed using some of the new GCMs in upcoming CMIP phases, which we hope will better reproduce the observed ENSO nonlinearity. KHB17 pointed out that the La Niña-like warming might be related to the upper-ocean diffusivity and thermal stratification; improving these upper-ocean properties might solve the problems of the unrealistic nonlinearity evident in most CMIP5 models. Some recent studies also support our notion that the ENSO nonlinearity is important for future projections of the mean-state SST patterns (Yeh and Kirtman 2007; Karamperidou et al. 2017).

- 5) Even for a first-order problem, “warmer minus control” is not necessarily a good analog of a gradual global warming.

Our results show that the La Niña-like warming happens only when the greenhouse forcing is increased gradually (Fig. 9). In the abrupt increase of CO₂, the warming response is more like a zonally uniform warming, because of the influence of a slow El Niño-like response in addition to the transient NEWS mechanism (Fig. 11). Therefore, we should emphasize that warmer minus control, which is often used in global warming research, is not necessarily a good analog of a gradual global warming even for a first-order feature of GCMs, since the transient response could be different from the equilibrium response and depend on the rate of warming.

- 6) At least in GFDL-ESM2M, the ENSO amplitude variation appears to be a cause, rather than an effect, of the mean-state SST variation. Our argument, however, remains too speculative to determine the causality with certainty.

Interestingly, even if the mean climate experiences a zonally uniform warming (see the fifth conclusion), the nonlinear ENSO amplitude has no dependence on the mean-state SST change in a warmer climate (Figs. 2 and 5). Therefore, it could be possible to hypothesize that the ENSO amplitude variation in GFDL-ESM2M

may be a cause, rather than an effect, of the mean-state SST variation.

We must admit, however, that our argument about the causality in GFDL-ESM2M remains uncertain (for alternative mechanisms, see also KHB17). Therefore, at this stage, what we would like to show in this particular study is as follows. We propose the NEWS mechanism, which can be simulated by an idealized model. We have detected some evidence to support the notion that GFDL-ESM2M (and maybe the real world) is influenced by NEWS. The importance of NEWS compared to other processes remains difficult to quantify, but NEWS is as plausible as some other processes, such as the ocean dynamical thermostat. Because the direction of causality is important for the NEWS mechanism to dominate the global warming response, further rigorous verifications are needed.

- 7) EENs might better be treated as a completely different phenomenon than the linear ENSO mode.

Some earlier studies regarded ENSO as a linear mode and predicted an increase of ENSO variance under global warming. If nonlinear ENSO dynamics are taken into account, however, one reaches the conclusion that ENSO variance should decrease. Because EENs have huge amplitudes compared to the linear ENSO mode, we expect the teleconnections to the extratropical regions should also be substantially different. For example, the area with SST warmer than 28°C (the threshold at which deep convection can occur in the current climate) is much larger in EENs. This large area cannot be described as a linear perturbation from the climatological mean, as suggested in Fig. 3. Many other features that have been believed to be typical for ENSO could be made radically different by the nonlinearity of EENs. Further investigation is needed to shed light on the abnormality of EENs compared to the known linear ENSO mode.

- 8) Understanding EENs may aid the understanding of Pacific multidecadal natural variability and change. NEWS-NECS cycle serves as one of many possibilities.

We have also introduced the opposite mechanism to NEWS, the nonlinear ENSO cooling suppression (NECS), by which “global cooling” suppresses the upwelling efficiency, excites EENs, and yields an El Niño-like cooling. Because a La Niña-like (El Niño like) mean state eventually cools (warms) Earth, the effect of NEWS can excite NECS, and vice versa. Though whether this NEWS-NECS cycle operates in the real world remains speculative, our idealized model and GFDL-ESM2M suggest that this NEWS-NECS cycle may partly contribute to the multidecadal

natural SST variability in the Pacific (Fig. 12), including the interdecadal Pacific oscillation (IPO), whose phase change is thought to be causally related to an occurrence of a large El Niño (e.g., Meehl et al. 2016) as the piControl run of GFDL-ESM2M suggests.

Some previous studies suggest that global warming hiatuses and slowdowns may be related to the multi-decadal variability of Pacific SSTs (e.g., Kosaka and Xie 2013, 2016). If the IPO can be partially explained by the NEWS–NECS cycle, then both atmospheric and oceanic roles must be important to understand the hiatuses in relation to nonlinear ENSO dynamics (Fig. 13). If the nonlinearity plays a role in producing the Pacific multidecadal variability, global warming hiatuses should be understood not as a unidirectionally forced response of the atmosphere to the “prescribed” SST variations but rather as two-way ocean–atmosphere interaction between the global mean atmospheric reservoir and the Pacific cold tongue. To realistically simulate global warming hiatuses, state-of-the-art GCMs may require further improvements to their ENSO nonlinearity.

Acknowledgments. The work was supported by the National Science Foundation (NSF) under Grant AGS-1549579 and Takenaka Scholarship Foundation. We thank Casey Hilgenbrink for reading the manuscript. Isaac Held’s blog post 45 (<http://www.gfdl.noaa.gov/blog/isaac-held/2014/04/24/45-dynamic-retardation-of-tropical-warming/>) was a useful reference for this study. We are also grateful to Tomoki Tozuka and three anonymous reviewers for their helpful comments and suggestions.

REFERENCES

- An, S.-I., and F.-F. Jin, 2000: An eigen analysis of the interdecadal changes in the structure and frequency of ENSO mode. *Geophys. Res. Lett.*, **27**, 2573–2576, doi:10.1029/1999GL011090.
- , and —, 2004: Nonlinearity and asymmetry of ENSO. *J. Climate*, **17**, 2399–2412, doi:10.1175/1520-0442(2004)017<2399:NAAOE>2.0.CO;2.
- , Y.-G. Ham, J.-S. Kug, F.-F. Jin, and I.-S. Kang, 2005: El Niño–La Niña asymmetry in the Coupled Model Intercomparison Project simulations. *J. Climate*, **18**, 2617–2627, doi:10.1175/JCLI3433.1.
- , J.-W. Kim, S.-H. Im, B.-M. Kim, and J.-H. Park, 2012: Recent and future sea surface temperature trends in tropical Pacific warm pool and cold tongue regions. *Climate Dyn.*, **39**, 1373–1383, doi:10.1007/s00382-011-1129-7.
- Andrews, T., J. M. Gregory, M. J. Webb, and K. E. Taylor, 2012: Forcing, feedbacks and climate sensitivity in CMIP5 coupled atmosphere–ocean climate models. *Geophys. Res. Lett.*, **39**, L09712, doi:10.1029/2012GL051607.
- Atwood, A. R., D. S. Battisti, A. T. Wittenberg, W. H. G. Roberts, and D. J. Vimont, 2017: Characterizing unforced multi-decadal variability of ENSO: A case study with the GFDL CM2.1 coupled GCM. *Climate Dyn.*, doi:10.1007/s00382-016-3477-9, in press.
- Battisti, D. S., and A. C. Hirst, 1989: Interannual variability in a tropical atmosphere–ocean model: Influence of the basic state, ocean geometry and nonlinearity. *J. Atmos. Sci.*, **46**, 1687–1712, doi:10.1175/1520-0469(1989)046<1687:IVIATA>2.0.CO;2.
- Behringer, D., and Y. Xue, 2004: Evaluation of the global ocean data assimilation system at NCEP: The Pacific Ocean. *Proc. Eighth Symp. on Integrated Observing and Assimilation Systems for Atmosphere, Oceans, and Land Surface*, Seattle, WA, Amer. Meteor. Soc., 2.3. [Available online at https://ams.confex.com/ams/84Annual/techprogram/paper_70720.htm.]
- Bellenger, H., É. Guilyardi, J. Leloup, M. Lengaigne, and J. Vialard, 2014: ENSO representation in climate models: From CMIP3 to CMIP5. *Climate Dyn.*, **42**, 1999–2018, doi:10.1007/s00382-013-1783-z.
- Boullanger, J.-P., C. Menkes, and M. Lengaigne, 2004: Role of high- and low-frequency winds and wave reflection in the onset, growth and termination of the 1997–1998 El Niño. *Climate Dyn.*, **22**, 267–280, doi:10.1007/s00382-003-0383-8.
- Cane, M. A., A. C. Clement, A. Kaplan, Y. Kushnir, D. Pozdnyakov, R. Seager, S. E. Zebiak, and R. Murtugudde, 1997: Twentieth-century sea surface temperature trends. *Science*, **275**, 957–960, doi:10.1126/science.275.5302.957.
- Christensen, J., and Coauthors, 2013: Climate phenomena and their relevance for future regional climate change. *Climate Change 2013: The Physical Science Basis*, T. F. Stocker et al., Eds., Cambridge University Press, 1217–1308, doi:10.1017/CBO9781107415324.028.
- Clement, A. C., R. Seager, M. A. Cane, and S. E. Zebiak, 1996: An ocean dynamical thermostat. *J. Climate*, **9**, 2190–2196, doi:10.1175/1520-0442(1996)009<2190:AODT>2.0.CO;2.
- Collins, M., and Coauthors, 2005: El Niño- or La Niña-like climate change? *Climate Dyn.*, **24**, 89–104, doi:10.1007/s00382-004-0478-x.
- , and Coauthors, 2010: The impact of global warming on the tropical Pacific Ocean and El Niño. *Nat. Geosci.*, **3**, 391–397, doi:10.1038/ngeo868.
- Fedorov, A. V., and S. G. Philander, 2000: Is El Niño changing? *Science*, **288**, 1997–2002, doi:10.1126/science.288.5473.1997.
- Hansen, J., R. Ruedy, M. Sato, and K. Lo, 2010: Global surface temperature change. *Rev. Geophys.*, **48**, RG4004, doi:10.1029/2010RG000345.
- Held, I. M., and B. J. Soden, 2006: Robust responses of the hydrological cycle to global warming. *J. Climate*, **19**, 5686–5699, doi:10.1175/JCLI3990.1.
- , M. Winton, K. Takahashi, T. Delworth, F. Zeng, and G. K. Vallis, 2010: Probing the fast and slow components of global warming by returning abruptly to preindustrial forcing. *J. Climate*, **23**, 2418–2427, doi:10.1175/2009JCLI3466.1.
- Jin, F.-F., 1996: Tropical ocean–atmosphere interaction, the Pacific cold tongue, and the El Niño–Southern Oscillation. *Science*, **274**, 76–78, doi:10.1126/science.274.5284.76.
- , 1997: An equatorial ocean recharge paradigm for ENSO. Part I: Conceptual model. *J. Atmos. Sci.*, **54**, 811–829, doi:10.1175/1520-0469(1997)054<0811:AEORPF>2.0.CO;2.
- , 1998: A simple model for the Pacific cold tongue and ENSO. *J. Atmos. Sci.*, **55**, 2458–2469, doi:10.1175/1520-0469(1998)055<2458:ASMFTP>2.0.CO;2.
- , S.-I. An, A. Timmermann, and J. Zhao, 2003: Strong El Niño events and nonlinear dynamical heating. *Geophys. Res. Lett.*, **30**, 1120, doi:10.1029/2002GL016356.

- Karamperidou, C., F.-F. Jin, and J. L. Conroy, 2017: The importance of ENSO nonlinearities in tropical Pacific response to external forcing. *Climate Dyn.*, doi:10.1007/s00382-016-3475-y, in press.
- Kim, S. T., W. Cai, F.-F. Jin, A. Santoso, L. Wu, E. Guilyardi, and S.-I. An, 2014: Response of El Niño sea surface temperature variability to greenhouse warming. *Nat. Climate Change*, **4**, 786–790, doi:10.1038/nclimate2326.
- Knutson, T. R., and S. Manabe, 1995: Time-mean response over the tropical Pacific to increased CO₂ in a coupled ocean-atmosphere model. *J. Climate*, **8**, 2181–2199, doi:10.1175/1520-0442(1995)008<2181:TMROTT>2.0.CO;2.
- Kohyama, T., and D. L. Hartmann, 2016: Antarctic sea ice response to weather and climate modes of variability. *J. Climate*, **29**, 721–741, doi:10.1175/JCLI-D-15-0301.1.
- , —, and D. S. Battisti, 2017: La Niña-like mean-state response to global warming and potential oceanic roles. *J. Climate*, **30**, 4207–4225, doi:10.1175/JCLI-D-16-0441.1.
- Kosaka, Y., and S.-P. Xie, 2013: Recent global-warming hiatus tied to equatorial Pacific surface cooling. *Nature*, **501**, 403–407, doi:10.1038/nature12534.
- , and —, 2016: The tropical Pacific as a key pacemaker of the variable rates of global warming. *Nat. Geosci.*, **9**, 669–673, doi:10.1038/ngeo2770.
- Levine, A., F. F. Jin, and M. J. McPhaden, 2016: Extreme noise-extreme El Niño: How state-dependent noise forcing creates El Niño–La Niña asymmetry. *J. Climate*, **29**, 5483–5499, doi:10.1175/JCLI-D-16-0091.1.
- Liu, W., S.-P. Xie, and J. Lu, 2016: Tracking ocean heat uptake during the surface warming hiatus. *Nat. Commun.*, **7**, 10926, doi:10.1038/ncomms10926.
- Luo, Y., J. Lu, F. Liu, and W. Liu, 2015: Understanding the El Niño-like oceanic response in the tropical Pacific to global warming. *Climate Dyn.*, **45**, 1945–1964, doi:10.1007/s00382-014-2448-2.
- , —, —, and O. Garuba, 2017: The role of ocean dynamical thermostat in delaying the El Niño-like response over the equatorial Pacific to climate warming. *J. Climate*, **30**, 2811–2827, doi:10.1175/JCLI-D-16-0454.1.
- Meehl, G. A., H. Teng, and J. M. Arblaster, 2014: Climate model simulations of the observed early-2000s hiatus of global warming. *Nat. Climate Change*, **4**, 898–902, doi:10.1038/nclimate2357.
- , A. Hu, and H. Teng, 2016: Initialized decadal prediction for transition to positive phase of the interdecadal Pacific oscillation. *Nat. Commun.*, **7**, 11718, doi:10.1038/ncomms11718.
- Meinshausen, M., and Coauthors, 2011: The RCP greenhouse gas concentrations and their extensions from 1765 to 2300. *Climatic Change*, **109**, 213–241, doi:10.1007/s10584-011-0156-z.
- Murakami, H., R. Mizuta, and E. Shindo, 2012: Future changes in tropical cyclone activity projected by multi-physics and multi-SST ensemble experiments using the 60-km-mesh MRI-AGCM. *Climate Dyn.*, **39**, 2569–2584, doi:10.1007/s00382-011-1223-x.
- Rayner, N., D. E. Parker, E. Horton, C. Folland, L. Alexander, D. Rowell, E. Kent, and A. Kaplan, 2003: Global analyses of sea surface temperature, sea ice, and night marine air temperature since the late nineteenth century. *J. Geophys. Res.*, **108**, 4407, doi:10.1029/2002JD002670.
- Smith, T. M., R. W. Reynolds, T. C. Peterson, and J. Lawrimore, 2008: Improvements to NOAA’s historical merged land-ocean surface temperature analysis (1880–2006). *J. Climate*, **21**, 2283–2296, doi:10.1175/2007JCLI2100.1.
- Taylor, K. E., R. J. Stouffer, and G. A. Meehl, 2012: An overview of CMIP5 and the experiment design. *Bull. Amer. Meteor. Soc.*, **93**, 485–498, doi:10.1175/BAMS-D-11-00094.1.
- Timmermann, A., J. Oberhuber, A. Bacher, M. Esch, M. Latif, and E. Roeckner, 1999: Increased El Niño frequency in a climate model forced by future greenhouse warming. *Nature*, **398**, 694–697, doi:10.1038/19505.
- , F.-F. Jin, and J. Abshagen, 2003: A nonlinear theory for El Niño bursting. *J. Atmos. Sci.*, **60**, 152–165, doi:10.1175/1520-0469(2003)060<0152:ANTFEN>2.0.CO;2.
- Urban, F. E., J. E. Cole, and J. T. Overpeck, 2000: Influence of mean climate change on climate variability from a 155-year tropical Pacific coral record. *Nature*, **407**, 989–993, doi:10.1038/35039597.
- Vecchi, G. A., and B. J. Soden, 2007: Global warming and the weakening of the tropical circulation. *J. Climate*, **20**, 4316–4340, doi:10.1175/JCLI4258.1.
- Waliser, D. E., and N. E. Graham, 1993: Convective cloud systems and warm-pool sea surface temperatures: Coupled interactions and self-regulation. *J. Geophys. Res.*, **98**, 12 881–12 893, doi:10.1029/93JD00872.
- Wang, B., and S.-I. An, 2001: Why the properties of El Niño changed during the late 1970s. *Geophys. Res. Lett.*, **28**, 3709–3712, doi:10.1029/2001GL012862.
- , and —, 2002: A mechanism for decadal changes of ENSO behavior: Roles of background wind changes. *Climate Dyn.*, **18**, 475–486, doi:10.1007/s00382-001-0189-5.
- Watanabe, M., H. Shioyama, H. Tatebe, M. Hayashi, M. Ishii, and M. Kimoto, 2014: Contribution of natural decadal variability to global warming acceleration and hiatus. *Nat. Climate Change*, **4**, 893–897, doi:10.1038/nclimate2355.
- Xie, S.-P., C. Deser, G. A. Vecchi, J. Ma, H. Teng, and A. T. Wittenberg, 2010: Global warming pattern formation: Sea surface temperature and rainfall. *J. Climate*, **23**, 966–986, doi:10.1175/2009JCLI3329.1.
- Yeh, S.-W., and B. P. Kirtman, 2007: ENSO amplitude changes due to climate change projections in different coupled models. *J. Climate*, **20**, 203–217, doi:10.1175/JCLI4001.1.
- Ying, J., P. Huang, and R. Huang, 2016: Evaluating the formation mechanisms of the equatorial Pacific SST warming pattern in CMIP5 models. *Adv. Atmos. Sci.*, **33**, 433–441, doi:10.1007/s00376-015-5184-6.
- Yokoi, S., and Y. N. Takayabu, 2009: Multi-model projection of global warming impact on tropical cyclone genesis frequency over the western North Pacific. *J. Meteor. Soc. Japan*, **87**, 525–538, doi:10.2151/jmsj.87.525.
- Zebiak, S. E., and M. A. Cane, 1987: A model El Niño–Southern Oscillation. *Mon. Wea. Rev.*, **115**, 2262–2278, doi:10.1175/1520-0493(1987)115<2262:AMENO>2.0.CO;2.
- Zheng, X.-T., S.-P. Xie, L.-H. Lv, and Z.-Q. Zhou, 2016: Intermodel uncertainty in ENSO amplitude change tied to Pacific Ocean warming pattern. *J. Climate*, **29**, 7265–7279, doi:10.1175/JCLI-D-16-0039.1.